Modification of the histone tetramer at the H3-H3 interface impacts tetrasome conformations and dynamics

Ordu, Orkide; Kremser, Leopold; Lusser, Alexandra; Dekker, Nynke H.

DOI
10.1063/1.5009100

Publication date
2018

Document Version
Accepted author manuscript

Published in
Journal of Chemical Physics

Modification of the Histone Tetramer at the H3-H3 Interface Impacts Tetrasome Conformations and Dynamics

Orkide Ordu[1], Leopold Kremser[2], Alexandra Lusser[3], and Nynke H. Dekker[1,*]

[1]Bionanoscience Department, Kavli Institute of Nanoscience, Delft University of Technology, Van der Maasweg 9, 2629 HZ Delft, The Netherlands
[2]Division of Clinical Biochemistry, Biocenter, Medical University of Innsbruck, Innrain 80, 6020 Innsbruck, Austria
[3]Division of Molecular Biology, Biocenter, Medical University of Innsbruck, Innrain 80-82, 6020 Innsbruck, Austria

*To whom correspondence should be addressed. Tel: +31(0)152783219; Fax: +31(0)152781202; Email: N.H.Dekker@tudelft.nl

ABSTRACT

Nucleosomes consisting of a short piece of deoxyribonucleic acid (DNA) wrapped around an octamer of histone proteins form the fundamental unit of chromatin in eukaryotes. Their role in DNA compaction comes with regulatory functions that impact essential genomic processes such as replication, transcription, and repair. The assembly of nucleosomes obeys a precise pathway in which tetramers of histones H3 and H4 bind to the DNA first to form tetrasomes, and two dimers of histones H2A and H2B are subsequently incorporated to complete the complex. As viable intermediates, we previously showed that tetrasomes can spontaneously flip between a left-handed and right-handed conformation of DNA-wrapping. To pinpoint the underlying mechanism, here we investigated the role of the H3-H3 interface for tetramer flexibility in the flipping process at the single-molecule level. Using Freely-Orbiting Magnetic Tweezers, we studied the assembly and structural dynamics of individual tetrasomes modified at the cysteines close to this interaction interface by iodoacetamide (IA) in real time. While such modification did not affect the structural properties of the tetrasomes, it caused a 3-fold change in their flipping kinetics. The results indicate that the IA-modification enhances the conformational plasticity of tetrasomes. Our findings suggest that subnucleosomal dynamics may be employed by chromatin as an intrinsic and adjustable mechanism to regulate DNA supercoiling.

I. INTRODUCTION

The genome of eukaryotic organisms is tightly packed into chromatin, a hierarchical deoxyribonucleic acid (DNA)-protein assembly with a repeating basic unit termed the nucleosome[1-3]. This fundamental complex consists of 147 base pairs (bp) of deoxyribonucleic acid (DNA) wrapped around a discoidal core of eight histone proteins by 1.7 turns in a left-handed superhelix[4-6]. The histone octamer comprises two copies of each of the core histones H2A, H2B, H3, and H4, which group into two types of heterodimers by the pairing of histones H2A and H2B, and histones H3 and H4, respectively[7, 8]. Via the four-helix region formed by both

H3 histones, the two H3-H4 dimers form a tetramer to which H2A/H2B dimers attach through similar interactions between histones H2B and H4. In the presence of DNA, the $(H3\text{-}H4)_2$ tetramer assembles first into a tetrasome, after which two H2A/H2B dimers bind to form the full nucleosome[9]. In cells, nucleosome assembly is promoted by histone chaperones such as Nucleosome Assembly Protein-1 (NAP1) or Chromatin Assembly Factor-1 (CAF1), and energy dependent chromatin assembly factors such as Adenosine triphosphate (ATP)-utilizing Chromatin assembly and remodeling Factor (ACF) or Chromodomain Helicase DNA binding protein-1 (CHD1)[10, 11]. *In vitro*, nucleosomes are reconstituted via salt-dialysis or using purified recombinant enzymes[12]. This first level of DNA compaction already highly affects, and thereby regulates the accessibility of the genome during vital processes such as replication, transcription, and repair. Therefore, detailed knowledge of nucleosome structure and dynamics is crucial for understanding cell function and viability.

Over four decades of research, structural and biochemical approaches have provided profound insights into the structure and function of nucleosomes[13-17]. More recently, such knowledge has been complemented by single-molecule studies which especially yielded substantial information concerning the dynamics of nucleosomes on the molecular scale[18]. It is now known that nucleosomes are intrinsically dynamic by partially un- and rewrapping their DNA ends (breathing[19-22]) and transiently opening the two turns of DNA along the axis of the superhelix (gaping[23]). In addition, nucleosome composition, stability and dynamics are altered by chemical modification of the histones (post-translational modifications[24]) and by active remodeling enzymes (ATP-dependent remodelers[25]). Furthermore, changes in nucleosome structure and dynamics are induced and regulated by the incorporation of histone variants with DNA-sequence or cell-cycle dependent expression, depositioning and specific functions[26, 27]. Under extraneous causes in the form of force, torque or changes in buffer conditions, nucleosomes undergo structural rearrangements resulting in different conformations[28]. In agreement with the stepwise assembly of nucleosomes, tetrasomes – consisting of 80 bp DNA wrapped around the $(H3\text{-}H4)_2$ tetramer (**Fig. 1(a),(b)**) – have been observed as stable intermediates in various studies[29-41]. Remarkably, tetrasomes have further been found to wrap DNA either in a left-handed or right-handed superhelix[42-47] (**Fig. 1(c)**). Recently, we have investigated this phenomenon by examining the dynamics of individual tetrasomes containing either the canonical *Drosophila* histone H3.1[48] or its main replacement variant H3.3[49]. By directly measuring the DNA linking number, we observed spontaneous flipping of such tetrasomes between a predominant state of left-handed superhelix, like in the full nucleosome, and a less occupied right-handed conformation of DNA-wrapping. The transition between the two states has been suggested to arise from the spontaneous reorientation of the $(H3\text{-}H4)_2$ tetramer at the H3-H3 interface. However, experiments directed at pinpointing the mechanism underlying the handedness dynamics of tetrasomes via real-time measurements have been lacking.

In this work, we investigated the potential role of flexibility at the H3-H3 interface of the histone tetramers in the handedness flipping of tetrasomes at the single-molecule level. Using Freely-Orbiting Magnetic Tweezers (FOMT[50]), we studied the assembly and structural dynamics of individual NAP1-loaded, chemically modified $(H3.1\text{-}H4)_2$ and $(H3.3\text{-}H4)_2$ tetrasomes in real time. The $(H3\text{-}H4)_2$ tetramers were treated with iodoacetamide (IA), which covalently binds to the

sulphur atom of the single cysteine at position 110 of the H3 histones (**Fig. 1(d)**). In a previous bulk study, this modification was found to form inherently left-handed tetrasomes and to block their transition to the right-handed conformation, potentially by generating a steric hindrance at the H3-H3 interface of the $(H3\text{-}H4)_2$ tetramers[44]. While IA-treated tetrasomes assembled with a very similar structure to untreated tetrasomes, we surprisingly found that the IA-treatment did not fully prevent the handedness flipping. However, the kinetics of IA-treated tetrasomes differed by 1.5-fold altered dwell times in the states of left-handed and right-handed DNA wrapping and by a 3-fold decrease of their ratio. These results indicate that the IA-treatment impacts the conformational flexibility and dynamics of tetrasomes. Our findings further suggest subnucleosomal dynamics as an intrinsic and tunable mechanism of chromatin to facilitate and regulate the impact of forces and torques on the genome. In the cell, such a mechanism could assist the corresponding activities by genome-processing enzymes such as the RNA polymerase[51], and could be adjusted by histone core modifications that alter histone-DNA or histone-histone interactions[52].

II. MATERIALS AND METHODS

A. Materials

1. Preparation of DNA constructs

Linear double-stranded DNA fragments of 1.97 kilo-base pairs (kbp) length were used as templates for tetrasome assembly in all experiments. This DNA fragment was generated by Polymerase Chain Reaction (PCR) from plasmid pBluescript (pBlue) 2,3 using primers 1 and 2 (**Table SI** of the **supplementary material**). Subsequently, shorter fragments (handles) of 643 bp length containing nucleotides modified by either multiple biotin (Roche Diagnostics, Basel, Switzerland) or multiple digoxigenin (Roche Diagnostics) linkages were ligated to either end of the main DNA fragment at BsaI restriction sites. These handles were amplified by PCR from pBlueSKII$^+$ (Stratagene/Agilent Technologies, Santa Clara, CA, United States) using primers 3 and 5 or 4 and 5 (**Table SI** of the **supplementary material**) in the presence of biotin-16-dUTP (Roche Diagnostics) or digoxigenin-11-dUTP (Roche Diagnostics) in a ratio of 1:5 with dTTP (Promega, Madison, WI, United States). The resulting DNA molecules contained no nucleosome-positioning sequences (**Fig. S1** of the **supplementary material**).

2. Protein Expression and Purification

Expression and purification of recombinant *Drosophila* NAP1, histones H3.1-H4 and H3.3-H4 was performed as described in the respective previous studies[48, 49]. Example gel images of the histones after Sodium Dodecyl Sulfate Polyacrylamide Gel Electrophoresis (SDS-PAGE) are shown in **Fig. S2(a),(b)** of the **supplementary material**.

3. Histone Treatment with Iodoacetamide (IA)

Purified H3.1-H4 and H3.3-H4 histones were dialyzed overnight against a buffer containing 10 millimolar (mM) 4-(2-hydroxyethyl)-1-piperazineethane-sulfonic acid-KOH (Hepes-KOH, pH 7.6), 10 mM KCl, 1 mM ethylenediaminetetraacetic acid (EDTA), and 10% (v/v) glycerol (buffer A) with two buffer changes to remove dithiothreitol (DTT). Subsequently, the samples were incubated with 1 mM IA in buffer A for 3 hours (h) in the dark at room temperature (RT). Subsequently, IA was removed by overnight dialysis against buffer A with 1 mM DTT at 4 ºC with two changes of buffer. Aliquots of H3-H4 solutions at the different steps of treatment were analyzed by SDS-PAGE (**Fig. S2(a),(b)** of the **supplementary material**). IA was our reagent of choice because it allows for a robust and quantitative modification of histone H3 in a technically straightforward manner[43-45].

4. Mass Spectrometry Analysis of IA-treated Histones

The degree of derivatization of the core histones by incorporation of IA was quantified by mass spectrometry. The experimental procedure is detailed in the **supplementary material**, together with the results shown in **Fig. S2(c),(d)**. We found that all H3.1 histones (100%) and virtually all H3.3 histones (99.3%) were derivatized upon IA-treatment. The underlying chromatograms from High-performance Liquid Chromatography (HPLC) and MS2-spectra are shown in **Fig. S3** and **Fig. S4** of the **supplementary material**, respectively.

B. Methods

1. Tetrasome Reconstitution via Salt-dialysis

The capability of the histones to successfully load onto the DNA constructs designed for use in the single-molecule experiments was confirmed by reconstituting tetrasomes with both untreated and IA-treated tetrasomes using salt-gradient dialysis[53, 54]. The details of the employed protocol can be found in the **supplementary material**, together with the results shown in **Fig. S5**.

2. Sample Preparation for Tetrasome Assembly in Single-molecule Experiments

In single-molecule experiments, tetrasome assembly was performed in flow cells consisting of a channel cut into a double-layer of parafilm that was sandwiched between two coverglasses (24x60 mm/#1, Menzel-Gläser, Braunschweig, Germany). The details of the assembly and preparation of the flow cells are described in the **supplementary material**.
For the experiments with histones, the buffer was changed to the measurement buffer containing 50 mM KCl (Merck, Darmstadt, Germany), 25 mM Hepes-KOH (pH 7.5; Sigma-Aldrich, St. Louis, MO, United States), 0.1 mM EDTA, 0.1 mg/ml Bovine Serum Albumin (BSA; Sigma Aldrich) for passivation, 0.25% Polyethylene Glycol (PEG; Sigma-Aldrich) and 0.25% Polyvinyl Alcohol (PVA; Sigma-Aldrich) as crowding agents. These buffer conditions with a 10-fold higher concentration of crowding agents compared to our previous studies [48, 49] were employed in most of the experiments (n=13 out of N=15) to increase tetrasome stability, since tetrasomes had been observed to disassemble in the course of the first two experiments. For the NAP1-mediated assembly of tetrasomes, either 51 nanomolar (nM) of an equimolar solution of $H3.1_{IA}$-H4 histones or 54 nM of an equimolar solution of $H3.3_{IA}$-H4 histones were incubated with 192

nM NAP1 for 30 min on ice in a buffer containing 50 millimolar (mM) KCl, 25 mM Hepes-KOH, 0.1 mM EDTA, 1 mg/ml BSA, 0.25% PEG, and 0.25% PVA. The incubated protein solution was then diluted at least 1:100, and 100 µl of the diluted solution was flushed into the flow cell to achieve the controlled assembly of a few tetrasomes. Free proteins were not flushed out in most measurements due to the enhancing effect on tetrasome disassembly observed in the first two experiments. In our previous studies, the presence of NAP1 was found to affect neither the stability of tetrasomes nor the flipping dynamics for $(H3.1\text{-}H4)_2$ tetrasomes, but to slightly increase the flipping probability of $(H3.3\text{-}H4)_2$ tetrasomes[48, 49].

3. Magnetic Tweezers Instrumentation

The NAP1-mediated assembly of tetrasomes was measured by directly monitoring the length and linking number of single DNA molecules using FOMT[50]. The hardware of the magnetic tweezers setup used in this study is described in the **supplementary material**. The exerted force was calibrated for each experiment and amounted to values between 0.6 pN and 0.7 pN. All experiments were performed at RT (22 ºC).

4. Data Analysis

The acquired data were analyzed using custom-written scripts in Matlab (Mathworks, Natick, MA, United States) and its built-in functions. The traces were analyzed for stepwise changes (steps) in DNA length and linking number using a custom-written step-fitting algorithm that improves upon its previous version described in Ref. 55. In a subsequent analysis, steps coinciding in both time traces, and hence indicating assembly or disassembly of tetrasomes, were identified using these fits. The sizes of the coinciding steps in DNA length (N=71) and linking number (N=71) upon assembly and disassembly were then extracted as key quantities describing the structure of the tetrasomes.

The handedness dynamics was only analyzed in those parts of the time traces that had stable DNA length and linking number baseline, reflecting stably bound tetrasomes (N=34). By fitting a corresponding number of Gaussian functions to the linking number data between two subsequent coinciding steps (**Fig. 4(b)**), the handedness flipping was characterized in terms of the associated alteration in tetrasome structure (n=22). The differences between the mean values of these fits were used to determine the change in linking number upon flipping (N=26). The relative peak area ratios of the individual Gaussian fits yielded the probabilities for the tetrasomes to occupy the corresponding states.

For a more detailed picture of the handedness dynamics, the times a single assembled and flipping $(H3.1_{IA}\text{-}H4)_2$ tetrasome spent in the left-handed or right-handed state of DNA wrapping (dwell times) were analyzed using a custom-written algorithm based on Ref. 56. Smoothed linking number data from the corresponding time traces (N=4) were assigned to the two states with the help of a threshold zone set by the midpoint of the mean values and their standard deviation (STD) obtained from the Gaussian fits to the unfiltered data (**Fig. 4(b)**). The times between subsequent transitions from one state to the other, i.e. intersections with the midpoint, were considered as the dwell times in the corresponding states. All data sets assigned

to the left-handed state (*N*=195 for 3.4 s or *N*=76 for 18.4 s time averaging by filtering) and right-handed state (*N*=199 for 3.4 s or *N*=81 for 18.4 s time averaging) were combined and fitted by an exponential function to determine the mean dwell time in each conformation (**Fig. 5(a),(b)**). For comparison, dwell times in these traces were also determined using the recorded dwell times in the plateaus of the steps fitted by the step-fitting algorithm in a separate analysis (*N*=65 for the left-handed state, *N*=64 for the right-handed state). For a direct comparison to the behavior of untreated tetrasomes, we further re-analyzed the dwell times in the partial time traces (*N*=6) of one of our earlier experiments with untreated (H3.1-H4)$_2$ tetrasomes published in the related article[48], using the same custom-written algorithm and settings (*N*=158 for 3.4 s or *N*=69 for 18.4 s time averaging for the left-handed state, *N*=160 for 3.4 s and *N*=71 for 18.4 s time averaging for the right-handed state).

Further details of the data analysis are described in the **supplementary material**, together with the complementing results shown in **Fig. S6** and **Fig. S7**. Overall, it should be noted that the values of the results obtained here for the dynamics and kinetics of the tetrasomes are an upper boundary due to the finite bead response time. The errors stated on the mean values determined in this study correspond to 1 STD based on the underlying distributions, unless indicated otherwise. The errors of computed quantities were calculated by error propagation.

III. RESULTS

A. NAP1-mediated Assembly of Iodoacetamide(IA)-treated Tetrasomes Results in Proper Complexes

Modified tetrasomes were assembled by flushing IA-treated histone ((H3$_{IA}$-H4)$_2$) tetramers pre-incubated with NAP1 chaperones into a flow cell containing individually tethered DNA molecules without specific nucleosome-positioning sequences. The formation of tetrasomes was monitored in real-time by measuring the length and the linking number of a single DNA molecule using FOMT[50]. A magnetic bead-tethered DNA molecule is precisely aligned with the axis of the vertically oriented magnetic field generated by a cylindrical permanent magnet allowing controlled application of force without constraining the bead's rotational motion (**Fig. 2(a)**). In this study, constant stretching forces of 0.6-0.7 pN were applied, comparable to our previous studies with untreated tetrasomes[48, 49]. The assembly of tetrasomes upon flushing in histone/chaperone-complexes was reflected in stepwise decreases in both DNA length z (in micrometers (µm)) (**Fig. 2(b)**) and linking number Θ (in turns) (**Fig. 2(c)**) simultaneously. Histone tetramers or NAP1 alone did not interact with the DNA molecule under identical conditions (**Fig. S8** of the **supplementary material**).

For improved statistics, different numbers of tetrasomes were assembled in several experiments (*N*=15) by changing the protein concentration. For the same purpose, the results obtained for (H3.1$_{IA}$-H4)$_2$ and (H3.3$_{IA}$-H4)$_2$ tetrasomes were combined, as we previously found the properties of untreated (H3.1-H4)$_2$ and (H3.3-H4)$_2$ tetrasomes to be very similar[48, 49]. The total, simultaneous changes in DNA length Δz_{tot} and linking number $\Delta\Theta_{tot}$ upon assembly of different numbers of tetrasomes in several experiments follow a linear relation with a slope of

$\Delta z_{tot}/\Delta\Theta_{tot}$ = 33 ± 6 nm/turn (95% confidence interval for estimated values from a linear fit) (**Fig. 3(a)**). Interestingly, some of the total changes in DNA linking number were smaller than the value expected from their corresponding change in DNA length, suggesting the assembly of right-handed tetrasomes. Therefore, such results (n=5) were excluded from the fit. From the total changes, we determined that 11% (n=8) of all modified tetrasomes (N=74) assembled in the right-handed conformation. In contrast to untreated tetrasomes, 66% (n=49) of the assembled modified tetrasomes were found to disassemble in the course of the measurements, regardless of the NAP1/histone ratio employed (**Fig. S9** of the **supplementary material**), indicating their decreased stability. A destabilizing effect of the 10-fold higher concentration of crowding agents compared to our previous studies on tetrasomes[48, 49] seems unlikely given the observation that under the same conditions, untreated tetrasomes did not disassemble (**Fig. S10(a)** of the **supplementary material**).

While multiple IA-treated tetrasomes mostly assembled simultaneously as reflected in large steps, their disassembly mainly occurred in a one-by-one fashion, indicating proper formation of individual complexes rather than aggregates (**Fig. 3(b)**). A possible reason for this behavior could be a cooperative binding mechanism that leads to a simultaneous or faster assembly of individual IA-treated tetrasomes than we can experimentally resolve. The several individual changes in DNA length $\Delta z_{dis-/ass}$ (N=71) and linking number $\Delta\Theta_{dis-/ass}$ upon tetrasome assembly or disassembly (N=71) also follow a linear relation with a slope of $\Delta z_{dis-/ass}/\Delta\Theta_{dis-/ass}$ = 26 ± 4 nm/turn (95% confidence interval on estimated values from a linear fit). Similar to the total changes, some of the changes in DNA linking number showed the opposite sign compared to those expected from the change in DNA length, indicating the assembly or disassembly of right-handed tetrasomes. Such data (n=14) were likewise excluded from the fit.

Combining the absolute values from all measurements with $(H3.1_{IA}\text{-}H4)_2$ and $(H3.3_{IA}\text{-}H4)_2$ tetrasomes for improved statistics yielded a mean change in DNA length of $\Delta z_{dis-/ass}$ = 28 ± 8 nm (n=49), and a mean change in linking number of $\Delta\Theta_{dis-/ass}$ = 1.0 ± 0.3 turns (n=61) upon the assembly or disassembly of IA-treated tetrasomes (**Fig. 3(c),(d)**). The individual distributions and results of the changes for the two types of tetrasomes are shown in **Fig. S11** and **Fig. S12** of the **supplementary material**. The mean values were determined from the data within the corresponding resolution limits and the contour length (50 nm) of nucleosomal DNA and the number of turns (1.7 turns) that it is wrapped around the histone octamer. Considering the above observed linear relation between the changes in DNA length and linking number, the mean values yield a ratio of $\Delta z_{dis-/ass}/\Delta\Theta_{dis-/ass}$ = 28 ± 12 nm/turn, which is in good agreement with the results obtained from the linear fits to the two different data sets above.

Overall, these values agree well with previous studies in which tetrasomes were characterized as intermediates during un- and refolding of complete nucleosomes[34-37] or by direct measurements[39, 40, 43-45, 47-49]. The linear dependency between the key quantities characterizing the structure of the modified tetrasomes further suggests that their conformation is independent of their number being assembled on a DNA molecule, as we previously observed for untreated tetrasomes as well. These results show that IA-treated tetrasomes assembled properly in our assay with a very similar structure to untreated tetrasomes.

B. IA-treated Tetrasomes Have Reduced Tendency Towards Handedness Flipping

To observe tetrasome behavior after assembly over an extended period of time, the FOMT experiments were carried out for several hours. As mentioned above, most modified tetrasomes were observed to disassemble in the course of the experiments, unlike untreated tetrasomes[48, 49]. On average, $(H3.1_{IA}\text{-}H4)_2$ tetrasomes were found to disassemble within 2499 ± 415 s (1 standard error of the mean (SEM), **Fig. S7** of the **supplementary material**). Therefore, the structural dynamics of tetrasomes was analyzed in partial traces with states of stable binding between two subsequent assembly and/or disassembly events. Quite unexpectedly, since IA-modification was previously reported to block the structural transition of tetrasomes[44], we found IA-treated tetrasomes to be dynamic in terms of their handedness. While the DNA length remained constant (**Fig. 4(a)**), the linking number of a DNA molecule loaded with a tetrasome continuously fluctuated between two states corresponding to a left-handed superhelix, like in the full nucleosome, and a right-handed conformation of DNA wrapping (**Fig. 4(b)**). Such handedness flipping was observed in 86% (n=12) of the analyzed partial traces (N=14) with $(H3.1_{IA}\text{-}H4)_2$ tetrasomes. $(H3.3_{IA}\text{-}H4)_2$ tetrasomes were found to flip in 50% (n=10) of the analyzed partial traces (N=20). The associated change in tetrasome structure was quantified by the difference between the means of the corresponding number of Gaussian distributions fitted to the linking number data that show flipping (N=26). On average, the change in DNA linking number associated with flipping $\Delta\Theta_{flipping}$ equalled 1.6 ± 0.2 turns (**Fig. 4(c)**), which exactly corresponds to the values obtained for the two types of tetrasomes individually (**Fig. S13** of the **supplementary material**). This value further agrees well with that determined previously for untreated tetrasomes and reaffirms our observation that IA-treated tetrasomes assembled into proper complexes.

Nevertheless, the considerable remaining fractions of the analyzed partial traces did not show such handedness flipping. This indicates the existence of another, rather metastable population/state induced upon IA-modification. Along these lines, we also observed that the linking number data of multiple loaded IA-treated tetrasomes never showed the number of states that would be expected, if they all flipped simultaneously. At most three states were observed in 14% (n=2) of the analyzed traces deduced from $(H3.1_{IA}\text{-}H4)_2$ tetrasomes, and in 10% (n=2) of the analyzed traces obtained with $(H3.3_{IA}\text{-}H4)_2$ tetrasomes. This implies that usually only one, but not necessarily the same tetrasome exhibited handedness flipping.

Additionally, in 43% of the data from experiments with $(H3.1_{IA}\text{-}H4)_2$ tetrasomes, the lowest linking number state did not correspond to the value expected for all tetrasomes being in the left-handed conformation. While not observed for $(H3.3_{IA}\text{-}H4)_2$ tetrasomes, this phenomenon indicates that some $(H3.1_{IA}\text{-}H4)_2$ tetrasomes also stably dwelled in the right-handed state. From the DNA length and the corresponding linking number values, we determined that 18% (n=6) of all assembled $(H3.1_{IA}\text{-}H4)_2$ tetrasomes (N=33) in the considered traces stably remained in the right-handed conformation.

Overall, these results show that IA-modification does not fully prevent tetrasomes from changing their handedness. Nonetheless, our findings clearly indicate that IA-treated

tetrasomes have a reduced tendency towards flipping, which might arise from the incorporated IA molecules. This would support the idea that a potential rotation of the two H3-H4 tetramers against each other at the H3-H3 interface is the mechanistic requirement enabling handedness flipping. The simultaneous flipping of multiple tetrasomes might be hindered by the increased stability of individual complexes in a cooperative setting. The differing behavior and statistics for $(H3.1_{IA}\text{-}H4)_2$ and $(H3.3_{IA}\text{-}H4)_2$ tetrasomes might result from subtle differences in their structure upon IA-incorporation. Similar to the case of tetrasome stability, the 10-fold higher concentration of crowding agents compared to our previous studies on tetrasomes[48, 49] is unlikely to affect tetrasome flipping, as untreated tetrasomes assembled in the same conditions did flip as previously observed (**Fig. S10(b)** of the **supplementary material**).

C. IA-treatment Impacts the Conformational Plasticity of Tetrasomes

The presence of non-flipping tetrasomes described above indicates that the H3-H3 interface of the histone tetramer plays an important role in tetrasome flexibility. However, since most IA-treated tetrasomes still exhibited handedness flipping, we looked more closely into its dynamics to obtain a more detailed picture of this process.

For this purpose, the linking number traces (N=4) of a single loaded, flipping $(H3.1_{IA}\text{-}H4)_2$ tetrasome were first analyzed in terms of the times that it spent in each state (dwell times). The underlying data analysis is described in **Materials and Methods** and the resulting mean dwell times of a $(H3.1_{IA}\text{-}H4)_2$ tetrasome in the left-handed and right-handed conformation are shown in **Fig. 5(a),(b)**, respectively. These values, and those determined in a separate analysis based on the dwell times from the step-fitting algorithm, together with the results obtained for an untreated $(H3.1\text{-}H4)_2$ tetrasome from the re-analysis of the partial traces of an earlier experiment[48] are summarized for comparison in **Table I**. While the total dwell times for each type of tetrasome varied depending on the smoothing, which in the case of the step-fitting algorithm is caused by missed events, their ratio was essentially not affected. This result suggests a reliable analysis that allows the direct comparison of the total dwell times obtained for an untreated tetrasome and an IA-treated tetrasome with the same settings, as well as their ratios.

Overall, a $(H3.1_{IA}\text{-}H4)_2$ tetrasome dwelled 1.5±0.3 times shorter in the left-handed state compared to an untreated $(H3.1\text{-}H4)_2$ tetrasome, while the opposite was the case for the right-handed state with a likewise longer dwell time. This indicates that left-handed and right-handed $(H3.1_{IA}\text{-}H4)_2$ tetrasomes are energetically less and more stable, respectively, than their untreated counterparts, while the transition barrier between the two states remains essentially unaffected. The overall impact of IA-treatment is clearly illustrated by the 3±1-fold decrease of the left- versus right-handed dwell time ratio, which suggests a change in the free energy difference between the two states of $(H3.1_{IA}\text{-}H4)_2$ and untreated $(H3.1\text{-}H4)_2$ tetrasomes.

The free energy difference between the two states can be determined from the ratio of the respective dwell times by computing $\Delta E = -\, k_B T \ln(\tau_{D,right}/\tau_{D,left})$. This calculation yields a value of $\Delta E_{IA} = 1.5 \pm 0.1\ k_B T$, which is considerably different from the values resulting from dwell time analysis for an untreated $(H3.1\text{-}H4)_2$ tetrasome, i.e. the previously reported value $\Delta E_0 = 2.6 \pm 0.8$

k_BT (Ref. 48) or the corresponding value ΔE_0 = 2.4 ± 0.1 k_BT determined via our updated analysis algorithm. Thus, the cumulative change in the free energy difference between the left-handed and right-handed state of IA-treated and unmodified tetrasomes by $\Delta E_0 - \Delta E_{IA}$ = 1.1 ± 0.3 k_BT is consistent with the 3±1-fold difference in the dwell time ratio.

For validation purposes, the same linking number data were also analyzed in terms of the probability for a $(H3.1_{IA}\text{-}H4)_2$ tetrasome to occupy either the left- or right-handed state. This was achieved by considering the peak areas of the fitted Gaussian distributions (**Fig. 4(b)**) whose relative ratios give the probabilities *p* and *1-p* to occupy the corresponding states. By this means, a single flipping $(H3.1_{IA}\text{-}H4)_2$ tetrasome was found to obtain the left-handed conformation with an average probability of p_{av} = 0.85 ± 0.11 (*N*=4), corresponding to an average probability of $1\text{-}p_{av}$ = 0.15 ± 0.11 for occupying the right-handed conformation. Likewise, the free energy difference between the two states of ΔE_{IA} = 1.7 ± 0.7 k_BT which is deduced from the ratio of the probabilities according to $\Delta E = -k_BT \ln((1-p)/p)$ is similar to the value obtained from the dwell time ratio above.

Alternatively, the free energy difference of the two states was also calculated from the probabilities of all data sets including multiple assembled $(H3.1_{IA}\text{-}H4)_2$ tetrasomes (N=12) by fitting to a binomial distribution (**Fig. 5(c)**). In this approach, the probabilities based on the relative peak area ratios of the Gaussian distributions for each data set with varying number of assembled tetrasomes were assigned to their corresponding states in terms of the number of tetrasomes being in the left-handed state. Non-observed states were assigned a probability of zero. These data were fit to a binomial distribution with the number of assembled tetrasomes, i.e. the expected number of states being fixed, and the probability of a tetrasome to have the left-handed conformation treated as the free parameter.
Averaging over all obtained values, yields a mean probability of p_{av} = 0.76 ± 0.15 of a $(H3.1_{IA}\text{-}H4)_2$ tetrasome to occupy the left-handed state. This value corresponds to a free energy difference between the two states of ΔE = 1.2 ± 0.6 k_BT which agrees well with the values determined from the two other approaches above. An untreated $(H3.1\text{-}H4)_2$ tetrasome, however, was previously found to occupy the left-handed conformation with a probability of p_{av} = 0.90 ± 0.08 (Ref. 48) corresponding to a free energy difference between the two states of ΔE_0 = 2.3 ± 0.8 k_BT (Ref. 48). Taken together, the results from different analysis approaches consistently indicate a decrease in the free energy difference between the states of left-handed and right-handed DNA wrapping in $(H3.1_{IA}\text{-}H4)_2$ versus $(H3.1\text{-}H4)_2$ tetrasomes by 1 k_BT.

For a $(H3.3_{IA}\text{-}H4)_2$ tetrasome, only the latter approach by fitting all probability data (*N*=10) to a binomial fit was used (**Fig. S14** of the **supplementary material**), because the structural dynamics of $(H3.3\text{-}H4)_2$ tetrasomes was previously observed to be very similar to $(H3.1\text{-}H4)_2$ tetrasomes and no dwell time data is available for direct comparison[49]. On average, a mean probability of p_{av} = 0.88 ± 0.08 was found for a $(H3.3_{IA}\text{-}H4)_2$ tetrasome to be in the left-handed state, which corresponds to a difference in free energy between the two states of ΔE_{IA} = 2.0 ± 0.7 k_BT. In contrast to the observation with $(H3.1_{IA}\text{-}H4)_2$ tetrasomes above, these values agree well with those obtained previously for untreated $(H3.3\text{-}H4)_2$ tetrasomes (p_{av} = 0.91 ± 0.03 and ΔE = 2.3 ± 0.4 k_BT (Ref. 49)). The differing results for $(H3.3_{IA}\text{-}H4)_2$ tetrasomes and $(H3.1_{IA}\text{-}H4)_2$ tetrasomes,

as also observed for their flipping behavior, might arise from subtle structural differences upon IA-incorporation. However, it was also observed that the handedness dynamics of $(H3.3\text{-}H4)_2$ tetrasomes was slightly stimulated by the presence of NAP1, in contrast to $(H3.1\text{-}H4)_2$ tetrasomes[48, 49]. In our experiments, NAP1 was present in solution throughout the measurements due to the observed trend of enhanced disassembly of IA-treated tetrasomes upon flushing out free proteins. Therefore, the mean probability and free energy difference for $(H3.3_{IA}\text{-}H4)_2$ tetrasomes might also be smaller than the obtained value and similar to those determined for $(H3.1_{IA}\text{-}H4)_2$ tetrasomes.

Overall, these results indicate that IA-modification influences the stability of and the kinetics between the two tetrasome conformations. The shorter dwell time in the left-handed state suggests its decreased stability, while the right-handed conformation with a dwell time increased to the same extent is more stable compared to untreated tetrasomes. These effects are also reflected by corresponding differences in the probabilities of finding an IA-treated tetrasome in a certain state. Thus, the IA-treatment results in a decrease of the free energy difference between the two states.

IV. DISCUSSION AND CONCLUSION

Since four decades, chromatin research continues to reveal various aspects of the structure, function, and dynamics of the nucleosome as the fundamental DNA-protein complex in increasing detail. The chemically, force-, or torque-induced partial or full removal of H2A/H2B dimers by changes in buffer conditions, mechanical manipulation, or by genome-processing enzymes such as the RNA polymerase[57-59], makes subnucleosomal structures a topic of great interest. As stable intermediates, tetrasomes were investigated early on by biochemical approaches[42, 43]. These pioneering experiments demonstrated the high affinity of the $(H3\text{-}H4)_2$ tetramers for either negatively or positively supercoiled DNA, resulting in mutually convertible tetrasome conformations of a left-handed superhelix, like in the full nucleosome, or a right-handed DNA wrapping, respectively. Additional studies have suggested that this transition in tetrasome handedness results from the spontaneous reorientation of the $(H3\text{-}H4)_2$ tetramer at the H3-H3 interface[44-47]. Our previous studies of the assembly and structural dynamics of tetrasomes at single-molecule level have confirmed the existence of two handedness states and revealed their dynamic nature[48, 49]. The tetrasomes were observed to continuously flip between a predominant left-handed and a less occupied right-handed conformation. However, these studies did not directly investigate the underlying mechanism of this phenomenon.

In this work, we sought to address this issue by interfering with the potential flexibility of the histone tetramer at the H3-H3 interface and monitoring the effects at the single-molecule level. We have investigated the NAP1-mediated assembly and structural dynamics of individual $(H3.1\text{-}H4)_2$ and $(H3.3\text{-}H4)_2$ tetrasomes modified with iodoacetamide (IA) at the single cysteine at position 110 of the H3 histones in real time using FOMT[50]. In biochemical analyses of bulk tetrasome assemblies, this modification was previously found to block the handedness flipping of tetrasomes by potentially generating a steric hindrance at the H3-H3 interface of the histone tetramers[44]. The IA-treated histone ($(H3_{IA}\text{-}H4)_2$) tetramers had been reported to only form

inherently left-handed tetrasomes lacking the structural transition to the right-handed conformation. In agreement with this biochemical study, IA-treated tetrasomes assembled with a similar structure to untreated tetrasomes in our assay, which indicates the formation of proper complexes. However, in contrast to untreated tetrasomes, we observed IA-treated tetrasomes to disassemble in the course of the experiments, which suggests their decreased stability, possibly due to changes in their properties upon IA-incorporation. In the previous biochemical analyses, IA-treated tetramers have also been found to exhibit a low affinity to relaxed circular DNA templates and modified tetrasomes migrated faster on a gel than untreated tetrasomes. However, unlike the observation of only left-handed IA-treated tetrasomes in that study, we found $(H3_{IA}\text{-}H4)_2$ tetramers to also form right-handed tetrasomes. The varying results likely arise from the use of different approaches: single-molecule experiments, performed in highly diluted conditions, are known to be more sensitive than bulk assays, especially in terms of revealing transient intermediates and the dynamics of biomolecules. Another reason for this discrepancy could be the difference in the topology of the employed DNA constructs, which might be critical. The different topological restriction of tethered linear DNA fragments being subject to – low – force in our assay and of supercoiled circular DNA molecules employed in the biochemical analyses might bias tetrasome assembly. Likewise, apart from right-handed assembly, we also observed IA-treated tetrasomes to exhibit spontaneous changes in their handedness. However, while their structural rearrangement upon handedness flipping was very similar to that of untreated tetrasomes, the kinetics were found to be different.

The different kinetics and energetics between IA-treated and untreated tetrasomes are shown by the schematic energy diagram presented in **Fig. 5(d),** based on the here obtained results. Setting the barrial energy ($E_{barrier}$) to the same value for a common reference, the free energy of left-handed IA-treated tetrasomes ($\Delta E_{IA,left}$) is by a small amount higher than that for untreated tetrasomes ($\Delta E_{0,left}$), as reflected in the 1.5-fold decrease in the corresponding dwell time $\tau_{D,left}$. Conversely, the 1.5-fold increase in the dwell time $\tau_{D,right}$ indicates a likewise lower free energy of right-handed IA-treated tetrasomes. These differences indicate that IA-treated tetrasomes are slightly less stable in the left-handed state, and slightly more stable in the right-handed conformation than untreated tetrasomes due to the incorporated IA molecules. This effect might also play the central role in the 3-fold decreased ratio of the dwell times for IA-treated tetrasomes, which corresponds to a change in the free energy difference between the two states of 1 k_BT compared to untreated tetrasomes, as determined from three different approaches. Knowing the transition rates $k_{l\rightarrow r}$ and $k_{r\rightarrow l}$, related to the corresponding dwell times $\tau_{D,left}$ and $\tau_{D,right}$ by $k=1/\tau$, the height of the respective transition barriers can be calculated according to $\Delta G = - k_BT \ln(k/k_0)$ with the rate k_0 for spontaneous transitions in tetrasome structure at zero force. Considering a rate of $k_0 \sim 10^7$ s^{-1} based on the value of $\sim 3*10^6$ s^{-1} previously estimated for spontaneous structural transitions of full nucleosomes[60], the energy barrier for the transition from the left-handed to the right-handed state can be estimated to $\Delta G_{0,l\rightarrow r}$ ~21.3 k_BT for untreated, and to $\Delta G_{IA,l\rightarrow r}$ ~20.8 k_BT for $(H3.1_{IA}\text{-}H4)_2$ tetrasomes. The same calculation gives an estimate of $\Delta G_{0,r\rightarrow l}$ ~18.9 k_BT and $\Delta G_{IA,r\rightarrow l}$ ~19.3 k_BT for the transition from the right-handed to the left-handed state for untreated and $(H3.1_{IA}\text{-}H4)_2$ tetrasomes,

respectively. The results consistently indicate that the energies of the two states are altered, while the energy barrier for the structural transition of tetrasomes is essentially unaffected.

On the whole, our findings show that the IA-treatment did not affect the overall structural properties of tetrasomes but had some impact on their stability, flexibility, and dynamics. The unexpected occurrence of continuous handedness flipping and assembly of IA-treated tetrasomes into the right-handed conformation indicate that the incorporation of the IA molecules does not fully prevent these dynamics. Our results are directly comparable to our previous studies of untreated tetrasomes, as the same technique and essentially the same conditions have been used (**Table II**). Based on the observations in other single-molecule assays[61], we do not expect such low volume concentrations (<1%) of crowding agents to have a significant impact on the kinetics and energetics of the biological system under study. For this reason, we conclude that the observed changes in the energetics and flipping kinetics of tetrasomes are due to the IA-treatment. The results suggest that IA-modification enhances the conformational plasticity of tetrasomes, while their structural dynamics is affected to a lesser extent. Considering the very low forces of 0.6-0.7 pN employed in our experiments, possible contributions from other phenomena such as DNA flexibility, cannot be excluded.

In a broader context, our previous and current findings suggest the handedness dynamics of tetrasomes as an intrinsic and tunable mechanism of chromatin to regulate the impact of supercoiling on the genome at the nucleosomal level. Although tetrasomes have not yet been observed *in vivo*, their existence seems quite likely based on *in vivo* studies that have reported higher exchange and mobility of H2A and H2B histones compared to histones H3 and H4[62-64], as well as the involvement of chaperones or remodelers that specifically target histones H2A and H2B[65, 66]. Interestingly, these observations were made in transcriptionally active chromatin, indicating an important role of subnucleosomal structures during genome-processing by the RNA polymerase exerting forces and torques on the DNA[51]. The same would be expected for other key cellular processes such as replication and DNA repair[67, 68]. Subnucleosomal structures could facilitate and regulate these processes, especially due to their intrinsic dynamics which could further be adjusted by histone core modifications altering DNA-histone or histone-histone interactions[52]. Next to collecting more evidence for the existence of subnucleosomal structures, the key and challenging task will be to identify their structural, functional, and dynamic properties in molecular detail in order to advance our understanding of the mechanisms underlying chromatin structure and dynamics.

SUPPLEMENTARY MATERIAL

See supplementary material for further details.

ACKNOWLEDGMENTS

The authors would like to thank Dr. Theo van Laar for preparing the DNA constructs, Alexandra Wille for preparation of the histones, Dr. Jacob W. J. Kerssemakers for providing the improved step-fitting algorithm, and Dr. Herbert Lindner for discussions on the mass spectrometry

analysis. Additionally, the authors would like to acknowledge Dr. Rifka Vlijm, Dr. Cees Dekker, Dr. Mariana Köber, Dr. Richard Janissen, and Dr. Sam Leachman for insightful discussions. This was work was financially supported by the European Research Council (ERC) via a Consolidator Grant DynGenome (No:312221) to N.H.D and by the Austrian Science Fund (FWF) [START Y275-B12] to A.L.

REFERENCES

[1] R. D. Kornberg, Science **184** 868 (1974).
[2] A. L. Olins, and D. E. Olins, Science **183** 330 (1974).
[3] P. Oudet, M. Gross-Bellard, and P. Chambon, Cell **4** 281 (1975).
[4] T. J. Richmond, J. T. Finch, B. Rushton, D. Rhodes, and A. Klug, Nature **311** 532 (1984).
[5] K. Luger, A. W. Mäder, R. K. Richmond, D. F. Sargent, and T. J. Richmond, Nature **389** 251 (1997).
[6] C. A. Davey, D. F. Sargent, K. Luger, A. W. Maeder, and T. J. Richmond, J. Mol. Biol. **319** 1097 (2002).
[7] A. Klug, D. Rhodes, J. Smith, J. T. Finch, and J. O. Thomas, Nature **287** 509 (1980).
[8] G. Arents, R. W. Burlingame, B. C. Wang, W. E. Love, and E. N. Moudrianakis, Proc. Natl. Acad. Sci. U. S. A. **88** 10148 (1991).
[9] S. E. Polo, and G. Almouzni, Curr. Opin. Genet. Dev. **16** 104 (2006).
[10] J. K. Tyler, Eur. J. Biochem. **269** 2268 (2002).
[11] A. Lusser, D. L. Urwin, and J. T. Kadonaga, Nat. Struct. Mol. Biol. **12** 160 (2005).
[12] A. Lusser, and J. T. Kadonaga, Nat. Methods **1** 19 (2004).
[13] S. Khorasanizadeh, Cell **116** 259 (2004).
[14] B. Li, M. Carey, and J. L. Workman, Cell **128** 707 (2007).
[15] O. J. Rando, and H. Y. Chang, in *Annu. Rev. Biochem.* (Annual Reviews, Palo Alto, 2009), pp. 245.
[16] G. E. Zentner, and S. Henikoff, Nat. Struct. Mol. Biol. **20** 259 (2013).
[17] R. K. McGinty, and S. Tan, Chem. Rev. **115** 2255 (2015).
[18] O. Ordu, A. Lusser, and N. H. Dekker, Biophys. Rev. **8** 33 (2016).
[19] G. Li, M. Levitus, C. Bustamante, and J. Widom, Nat. Struct. Mol. Biol. **12** 46 (2005).
[20] W. J. A. Koopmans, A. Brehm, C. Logie, T. Schmidt, and J. van Noort, J. Fluoresc. **17** 785 (2007).
[21] A. Miyagi, T. Ando, and Y. L. Lyubchenko, Biochemistry **50** 7901 (2011).
[22] S. Wei, S. J. Falk, B. E. Black, and T. H. Lee, Nucleic Acids Res. **43** e111 (2015).
[23] T. T. Ngo, and T. Ha, Nucleic Acids Res. **43** 3964 (2015).
[24] G. D. Bowman, and M. G. Poirier, Chem. Rev. **115** 2274 (2015).
[25] C. R. Clapier, and B. R. Cairns, in *Annu. Rev. Biochem.* (Annual Reviews, Palo Alto, 2009), pp. 273.
[26] P. B. Talbert, and S. Henikoff, Nat. Rev. Mol. Cell Biol. **11** 264 (2010).
[27] P. B. Talbert, and S. Henikoff, Nat. Rev. Mol. Cell Biol. **18** 115 (2017).
[28] A. J. Andrews, and K. Luger, Annu. Rev. Biophys. **40** 99 (2011).
[29] B. Sollner-Webb, R. D. Camerini-Otero, and G. Felsenfeld, Cell **9** 179 (1976).
[30] M. Bina-Stein, and R. T. Simpson, Cell **11** 609 (1977).
[31] T. H. Eickbush, and E. N. Moudrianakis, Biochemistry **17** 4955 (1978).

[32] F. Dong, and K. E. Vanholde, Proc. Natl. Acad. Sci. U. S. A. **88** 10596 (1991).
[33] S. Jackson, W. Brooks, and V. Jackson, Biochemistry **33** 5392 (1994).
[34] B. D. Brower-Toland, C. L. Smith, R. C. Yeh, J. T. Lis, C. L. Peterson, and M. D. Wang, Proc. Natl. Acad. Sci. U. S. A. **99** 1960 (2002).
[35] G. J. Gemmen, R. Sim, K. A. Haushalter, P. C. Ke, J. T. Kadonaga, and D. E. Smith, J. Mol. Biol. **351** 89 (2005).
[36] S. Mihardja, A. J. Spakowitz, Y. L. Zhang, and C. Bustamante, Proc. Natl. Acad. Sci. U. S. A. **103** 15871 (2006).
[37] M. A. Hall, A. Shundrovsky, L. Bai, R. M. Fulbright, J. T. Lis, and M. D. Wang, Nat. Struct. Mol. Biol. **16** 124 (2009).
[38] V. Bohm, A. R. Hieb, A. J. Andrews, A. Gansen, A. Rocker, K. Toth, K. Luger, and J. Langowski, Nucleic Acids Res. **39** 3093 (2011).
[39] R. Vlijm, J. S. J. Smitshuijzen, A. Lusser, and C. Dekker, PLoS One **7**, e46306 11 (2012).
[40] A. J. Katan, R. Vlijm, A. Lusser, and C. Dekker, Small **11** 976 (2015).
[41] T. Elbel, and J. Langowski, J. Phys. Condens. Matter **27** 064105 (2015).
[42] V. Jackson, Biochemistry **34** 10607 (1995).
[43] A. Hamiche, V. Carot, M. Alilat, F. DeLucia, M. F. Odonohue, B. Revet, and A. Prunell, Proc. Natl. Acad. Sci. U. S. A. **93** 7588 (1996).
[44] A. Hamiche, and H. Richard-Foy, J. Biol. Chem. **273** 9261 (1998).
[45] M. Alilat, A. Sivolob, B. Revet, and A. Prunell, J. Mol. Biol. **291** 815 (1999).
[46] A. Sivolob, and A. Prunell, J. Mol. Biol. **295** 41 (2000).
[47] A. Sivolob, F. De Lucia, M. Alilat, and A. Prunell, J. Mol. Biol. **295** 55 (2000).
[48] R. Vlijm, M. Lee, J. Lipfert, A. Lusser, C. Dekker, and N. H. Dekker, Cell Rep. **10** 216 (2015).
[49] R. Vlijm, M. Lee, O. Ordu, A. Boltengagen, A. Lusser, N. H. Dekker, and C. Dekker, PLoS One **10** e0141267 (2015).
[50] J. Lipfert, M. Wiggin, J. W. J. Kerssemakers, F. Pedaci, and N. H. Dekker, Nature Communications **2**, 439 9 (2011).
[51] C. Lavelle, Curr. Opin. Genet. Dev. **25** 74 (2014).
[52] P. Tessarz, and T. Kouzarides, Nat. Rev. Mol. Cell Biol. **15** 703 (2014).
[53] K. Luger, T. J. Rechsteiner, and T. J. Richmond, Methods Enzymol. **304** 3 (1999).
[54] K.-M. Lee, and G. Narlikar, in *Curr. Protoc. Mol. Biol.* (John Wiley & Sons, Inc., 2001).
[55] J. W. J. Kerssemakers, E. L. Munteanu, L. Laan, T. L. Noetzel, M. E. Janson, and M. Dogterom, Nature **442** 709 (2006).
[56] J. Lipfert, G. M. Skinner, J. M. Keegstra, T. Hensgens, T. Jager, D. Dulin, M. Kober, Z. B. Yu, S. P. Donkers, F. C. Chou, R. Das, and N. H. Dekker, Proc. Natl. Acad. Sci. U. S. A. **111** 15408 (2014).
[57] J. L. Workman, and R. E. Kingston, Annu. Rev. Biochem. **67** 545 (1998).
[58] S. J. Petesch, and J. T. Lis, Trends Genet. **28** 285 (2012).
[59] S. S. Teves, C. M. Weber, and S. Henikoff, Trends Biochem. Sci. **39** 577 (2014).
[60] A. Bancaud, G. Wagner, N. Conde e Silva, C. Lavelle, H. Wong, J. Mozziconacci, M. Barbi, A. Sivolob, E. Le Cam, L. Mouawad, J. L. Viovy, J. M. Victor, and A. Prunell, Mol. Cell **27** 135 (2007).
[61] N. F. Dupuis, E. D. Holmstrom, and D. J. Nesbitt, Proc. Natl. Acad. Sci. U. S. A. **111** 8464 (2014).
[62] B. W. Baer, and D. Rhodes, Nature **301** 482 (1983).
[63] H. Kimura, and P. R. Cook, J. Cell Biol. **153** 1341 (2001).

[64] C. Thiriet, and J. J. Hayes, in *Chromatin Dynamics in Cellular Function*, edited by B. C. Laurent (Springer Berlin Heidelberg, Berlin, Heidelberg, 2006), pp. 77.
[65] D. Reinberg, and R. J. Sims, J. Biol. Chem. **281** 23297 (2006).
[66] M. Bruno, A. Flaus, C. Stockdale, C. Rencurel, H. Ferreira, and T. Owen-Hughes, Mol. Cell **12** 1599 (2003).
[67] L. J. Benson, Y. L. Gu, T. Yakovleva, K. Tong, C. Barrows, C. L. Strack, R. G. Cook, C. A. Mizzen, and A. T. Annunziato, J. Biol. Chem. **281** 9287 (2006).
[68] O. Gursoy-Yuzugullu, N. House, and B. D. Price, J. Mol. Biol. **428** 1846 (2016).
[69] C. R. Clapier, S. Chakravarthy, C. Petosa, C. Fernandez-Tornero, K. Luger, and C. W. Muller, Proteins **71** 1 (2008).
[70] L. Favrot, D. H. Lajiness, and D. R. Ronning, J. Biol. Chem. **289** 25031 (2014).

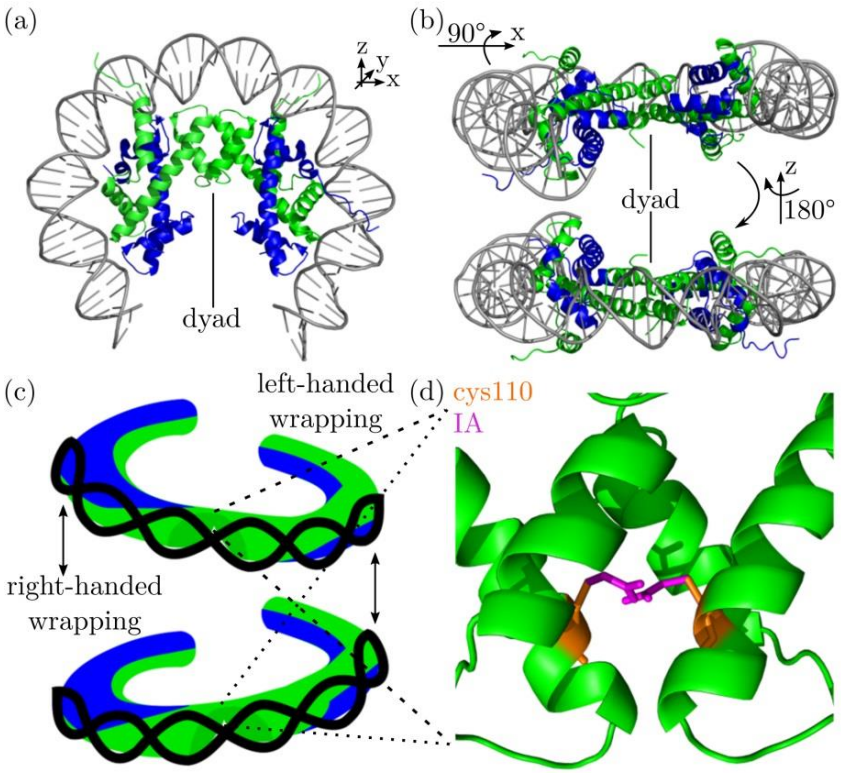

FIG. 1. Schematics of the tetrasome structure and associated changes in handedness. (a) Top view of 80 bp of DNA (gray) wrapped around a horseshoe-shaped protein complex containing the core histones H3 (green) and H4 (blue) in a left-handed superhelix. Two H3-H4 heterodimers form a tetramer through the central four-helix domain of the H3 histones. This image was generated by modifying the structural data of the *Drosophila* nucleosome from the Research Collaboratory for Structural Bioinformatics (RCSB) Protein Data Bank (PDB) with the identification code 2PYO[69] using the PyMOL Molecular Graphics System, Version 1.8.0.0 Schrödinger, LLC. **(b)** Side views of the structure in (a) along the pseudo-twofold symmetry (dyad) axis. **(c)** Illustration of the two possible ways of DNA-wrapping, left-handed or right-handed, around the tetramer. Flipping between these two tetrasome conformations may result from spontaneous reorientation of the heterodimers at the H3-H3 interface[43-45, 47-49]. **(d)** Zoomed-in structure of (a) at the H3-H3 interface that separates the H3-H4 heterodimers. Iodoacetamide (IA) treatment of the histones results in derivatization (magenta) of the cysteine at position 110 (orange) of both histones H3. This image was generated by further modifying the structural data of the *Drosophila* nucleosome with two copies of the IA molecule extracted from the structure with PDB identification code 4QDT[70] using PyMOL.

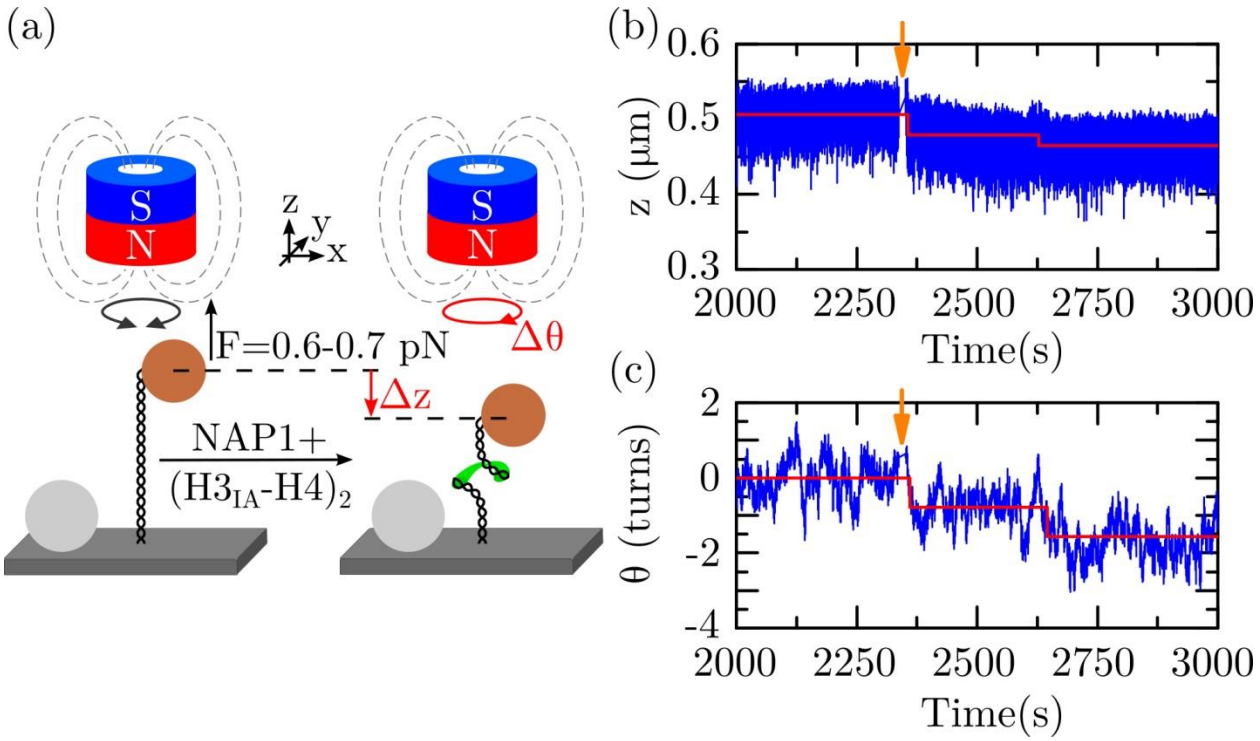

FIG. 2. Experimental configuration. (a) The assembly and structural dynamics of $(H3_{IA}\text{-}H4)_2$ tetrasomes were studied using FOMT[50]. A single DNA molecule (black) is tethered between the lower coverglass (dark gray) of a flow cell and a micron-sized paramagnetic bead (brown) that is subject to a constant force exerted by a permanent magnet (blue/red) of cylindrical geometry above the flow cell. The bead is free to rotate in the x,y-plane, which allows direct measurement of the twist in the DNA molecule in addition to its length. Non-magnetic beads (light gray) adhered to the surface are used as reference to correct for drift. Flushing in of $(H3_{IA}\text{-}H4)_2$ tetramers pre-incubated with the chaperone NAP1 results in the assembly of the modified tetrasomes, which is reflected in the decrease of the molecule's length Δz (red arrow) and linking number $\Delta\Theta$ (red circular arrow). **(b),(c)** Partial time traces of a DNA molecule's length z (in µm, (b)) and linking number Θ (in turns, (c)) simultaneously following the assembly of two $(H3.3_{IA}\text{-}H4)_2$ tetrasomes after flushing in the histone/chaperone complexes (indicated by orange arrows). The assembly of the modified tetrasomes happened in the form of consecutive, distinct steps that were detected using a custom-written step-fitting algorithm (red lines) (see **Materials and Methods** and **supplementary material**). Here, the two tetrasomes induced two simultaneous steps in both DNA length and linking number with the sizes Δz = 28 ± 8 nm/ $\Delta\Theta$ = -0.8 ± 0.3 turns, and Δz = 15 ± 8 nm/ $\Delta\Theta$ = -0.8 ± 0.3 turns, respectively (errors are 1 STD determined from the values of all experiments as described in the main text and **Fig. 3(c),(d)**).

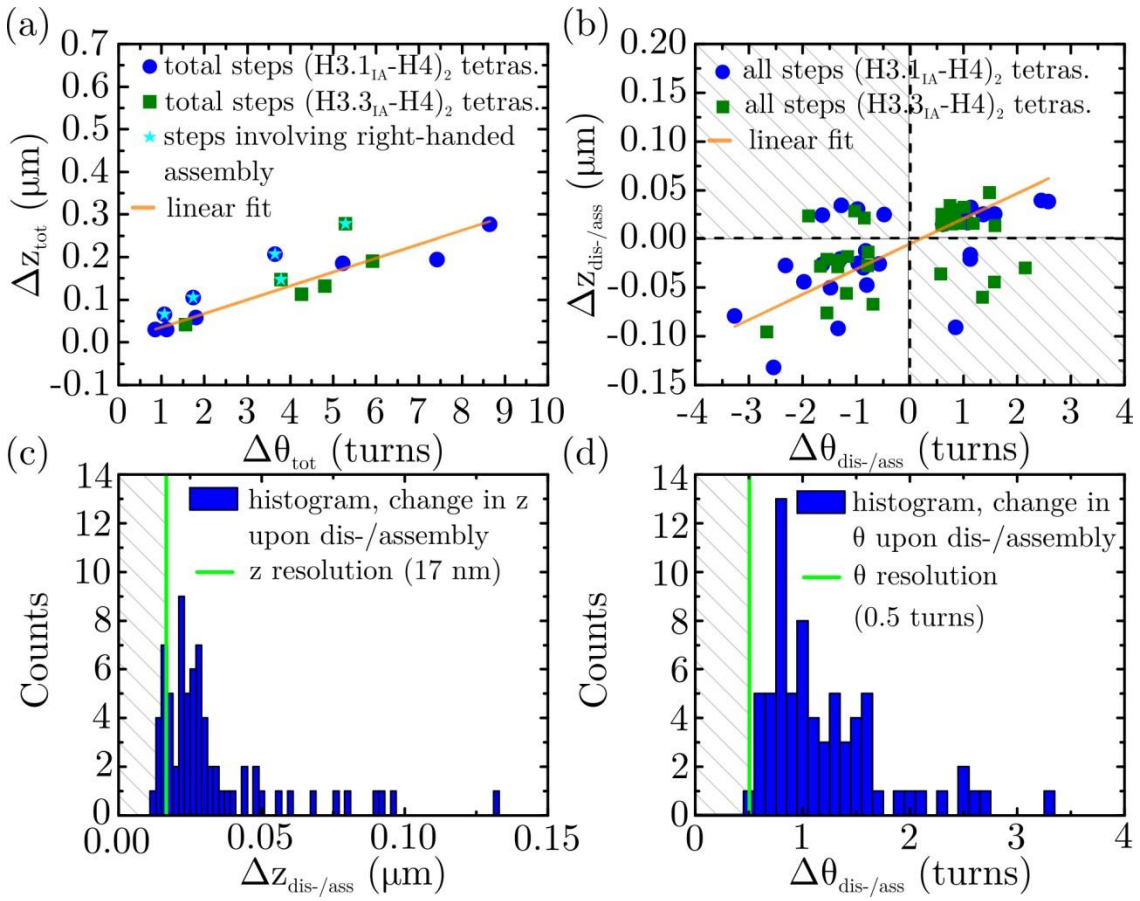

FIG. 3. Changes in DNA length and linking number upon disassembly/assembly of IA-treated tetrasomes. (a) Total changes in DNA length Δz_{tot} (in μm) upon assembly of different numbers of $(H3.1_{IA}\text{-}H4)_2$ (blue circles) or $(H3.3_{IA}\text{-}H4)_2$ tetrasomes (dark green squares) in several experiments plotted against their corresponding total change in DNA linking number $\Delta\Theta_{tot}$ (in turns) (N=15). A linear fit (orange solid line) yielded a slope of $\Delta z_{tot}/\Delta\Theta_{tot}$ = 33 ± 6 nm/turn (95% confidence interval for estimated values). Data involving right-handed assembly (cyan stars, n=5) were excluded from the fit (see main text). **(b)** Changes in DNA length $\Delta z_{dis-/ass}$ (in μm) upon disassembly/assembly of IA-treated tetrasomes plotted against their corresponding change in DNA linking number $\Delta\Theta_{dis-/ass}$ (in turns) (N=71). A linear fit yielded a slope of $\Delta z_{dis-/ass}/\Delta\Theta_{dis-/ass}$ = 26 ± 4 nm/turn (95% confidence interval for estimated values). Data involving right-handed dis-/assembly (shaded areas, n=14) were excluded from the fit (see main text). **(c)** Histogram of the changes in DNA length $\Delta z_{dis-/ass}$ (blue bars) upon disassembly/assembly of IA-treated tetrasomes plotted together with the mean spatial resolution based on 1 STD (17 nm, green line). The mean change in length of $\Delta z_{dis-/ass}$ = 28 ± 8 nm was determined from the data within the range bounded by the resolution limit (shaded area) and the DNA contour length wrapped in a full nucleosome (50 nm) (n=49). **(d)** Histogram of the changes in DNA linking number $\Delta\Theta_{dis-/ass}$ plotted together with the mean spatial resolution based on 1 STD (0.5 turns, green line). The mean change in linking number of $\Delta\Theta_{dis-/ass}$ = 1.0 ± 0.3 turns was determined from the data within the range bounded by the resolution limit (shaded area) and the number of turns the DNA is wrapped around the histone core in a full nucleosome (1.7 turns) (n=61).

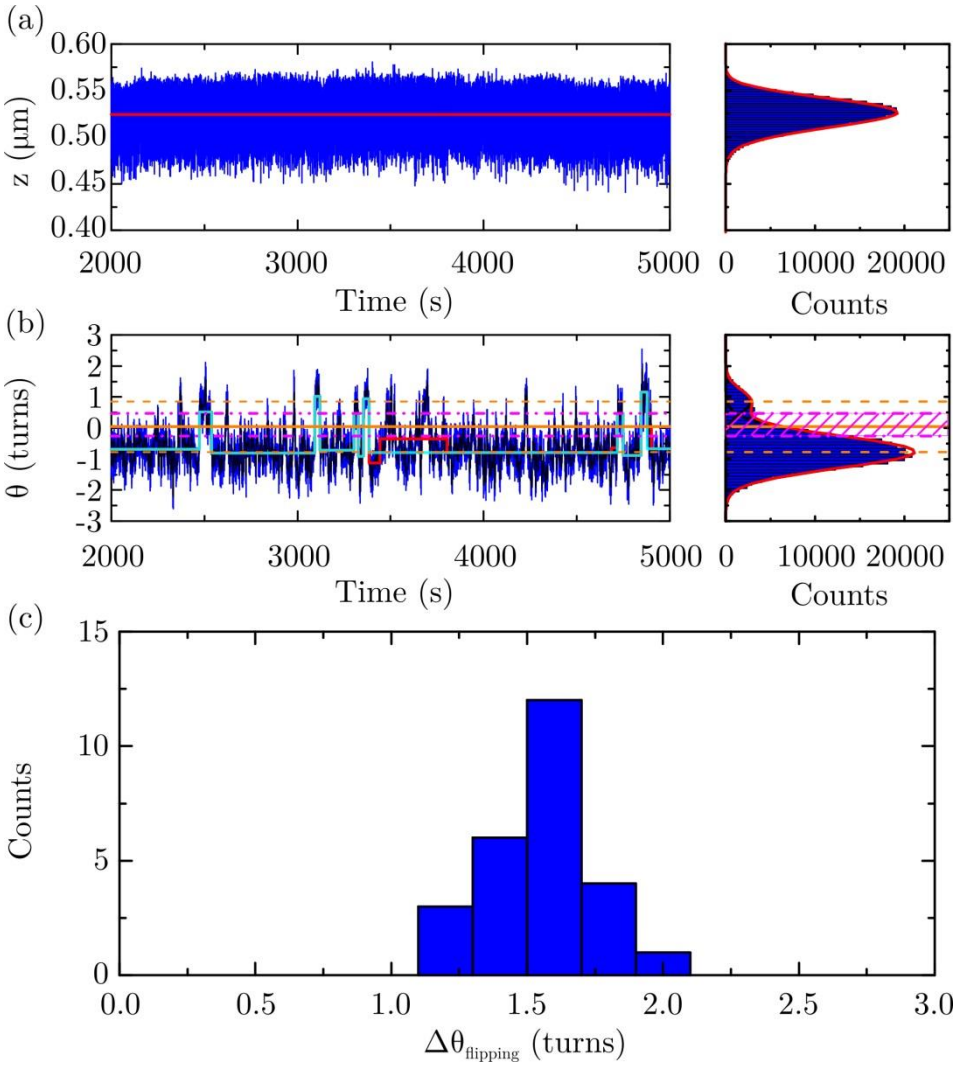

FIG. 4. Handedness flipping of IA-treated tetrasomes. (a) Partial time trace of a DNA molecule's length *z* (in μm) after the assembly of a $(H3.1_{IA}\text{-}H4)_2$ tetrasome. The DNA length stays constant over time, as can be seen both from the fit to the time trace (red line) by the custom-written step-fitting algorithm and its histogram on the right panel. The data for the histogram were fitted by a gamma function (red line in histogram) after mirroring at the x-axis and offsetting to positive values (see **supplementary material**). **(b)** The corresponding part of the time trace of the same DNA molecule's linking number *Θ* (in turns). This shows spontaneous fluctuations between a predominantly occupied left-handed state and a less occupied right-handed state with a mean of Θ_{left} = -0.77 ± 0.01 turns and Θ_{right} = +0.86 ± 0.06 turns (95% confidence intervals for estimated values; orange dashed lines), respectively, as can be seen both from the fit to the time trace (red line) by the custom-written step-fitting algorithm and its histogram on the right panel. The data for the histogram were fit to two Gaussian functions (black lines in the histogram) underlying the full profile (red line in the histogram). For dwell time analysis, the time trace was smoothed (black) before categorizing the data into the two states based on a threshold (orange solid line) set at the average value of the means determined from the unfiltered data (orange dashed lines). The threshold was further extended to a zone (magenta striped area) bounded by 1 STD from the corresponding means (magenta dashed-dotted lines). Alternatively, the dwell times in the step plateaus from the step-fitting algorithm were analyzed after manual correction to obtain a better match to the data (cyan solid line). **(c)** Histogram of the changes in linking number upon handedness flipping of IA-treated tetrasomes. The data has a mean value of $\Delta\Theta_{flipping}$ = 1.6 ± 0.2 turns (*N*=26).

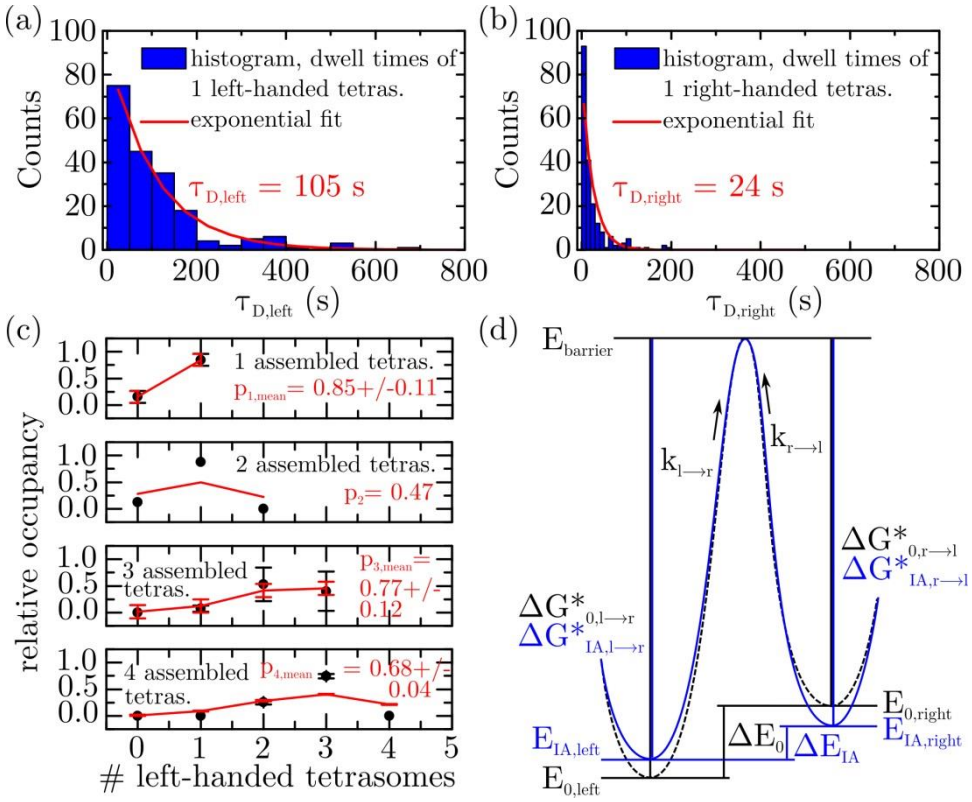

FIG. 5. Kinetics and energetics of IA-treated $(H3.1\text{-}H4)_2$ tetrasomes. (a) Histogram of the dwell times of a single $(H3.1_{IA}\text{-}H4)_2$ tetrasome in the left-handed state obtained from linking number time traces smoothed by averaging over N=340 data points, corresponding to a time average of 3.4 s, using a moving average filter. An exponential fit (red line) yielded a mean dwell time of $\tau_{D,left}$ = 105 +8/-7 s. **(b)** Histogram of the dwell times of a single $(H3.1_{IA}\text{-}H4)_2$ tetrasome in the right-handed state obtained from the same linking number data as described in (a). An exponential fit (red line) yielded a mean dwell time of $\tau_{D,right}$ = 24 ± 2 s. **(c)** Relative occupancies of the left-handed states obtained from the ratios of the mean peak areas of the linking number distributions for different numbers of assembled, flipping $(H3.1_{IA}\text{-}H4)_2$ tetrasomes. Data sets displaying the same number of assembled tetrasomes were averaged (black circles), if applicable, and plotted together with a corresponding binomial curve (red line) generated using the mean value of the probabilities obtained from a binomial fit to each data set. Data sets displaying different number of assembled tetrasomes are presented in separate panels. Non-occupied states were assigned to the value of 0 relative occupancy. A mean probability for a $(H3.1_{IA}\text{-}H4)_2$ tetrasome to occupy the left-handed state of p_{left} = 0.76 ± 0.15 was determined by averaging over all individual data sets. **(d)** Energy diagram of untreated (black) and $(H3.1_{IA}\text{-}H4)_2$ tetrasomes (blue) based on the values determined from the dwell times and the linking number distributions. While the free energy of left-handed $(H3.1_{IA}\text{-}H4)_2$ tetrasomes $E_{IA,left}$ is slightly higher, that of right-handed $(H3.1_{IA}\text{-}H4)_2$ tetrasomes $E_{IA,right}$ is slightly less by the same extent than the respective levels for untreated tetrasomes, $E_{0,left}$ and $E_{0,right}$. Likewise, the free energy difference ΔE_{IA} between the two states of $(H3.1_{IA}\text{-}H4)_2$ tetrasomes is less than that for untreated tetrasomes, ΔE_0. The energy barriers for the transitions between the two states with the rates $k_{l\to r}$ and $k_{r\to l}$, are, respectively, decreased and increased for IA-treated tetrasomes ($\Delta G_{IA,l\to r}$ and $\Delta G_{IA,r\to l}$) compared to the barriers for untreated tetrasomes, $\Delta G_{0,l\to r}$ and $\Delta G_{0,r\to l}$.

Table I. Results of the dwell time analysis. The dwell times $\tau_{D,left}$ in the left-handed state and $\tau_{D,right}$ right-handed state were obtained as described in **Materials and Methods.**

Sample	time average in filtering (s)	$\tau_{D,left}$ (s)	$\tau_{D,right}$ (s)	$\tau_{D,left}/\tau_{D,right}$
$(H3.1\text{-}H4)_2$ tetrasomes	3.4 (N=340)	177 +15/-12*	16 ± 1	11 ± 1*
"	18.4 (N=1840)	366 +51/-39*	29 +4/-3	13 ± 2*
$(H3.1_{IA}\text{-}H4)_2$ tetrasomes	3.4 (N=340)	105 +8/-7	24 ± 2	4 ± 0*
"	18.4 (N=1840)	244 +32/-25	52 +6/-5	5 ± 1*
"	step fitting algorithm	288 +41/-32	71 +10/-7	4 ± 1*

*errors calculated by error propagation

Table II. Summary of the properties of IA-treated and untreated tetrasomes for comparison.

Quantity	$(H3.1\text{-}H4)_2$ tetrasomes	$(H3.1_{IA}\text{-}H4)_2$ tetrasomes	$(H3.3\text{-}H4)_2$ tetrasomes	$(H3.3_{IA}\text{-}H4)_2$ tetrasomes
$\Delta z_{dis-/ass}$ (nm)	24 ± 3*	29 ± 8	25 ± 6**	26 ± 8
$\Delta\theta_{dis-/ass}$ (turns)	0.73 ± 0.05*	1.1 ± 0.3	0.8 ± 0.2**	1.0 ± 0.3
$\Delta\theta_{flipping}$ (turns)	1.7 ± 0.1*	1.6 ± 0.2	1.7 ± 0.1**	1.6 ± 0.2
$\tau_{D,left}$ (s)	177 +15/-12	105 +8/-7	-	-
$\tau_{D,right}$ (s)	16 ± 1	24 ± 2	-	-
$\Delta E_{dwell\text{-}times}$ (k_BT)	2.4 ± 0.1	1.5 ± 0.1	-	-
$\Delta E_{binomial\text{-}fits}$ (k_BT)	2.3 ± 0.8*	1.2 ± 0.6	2.3 ± 0.4** (1.6 ± 0.8**)	2.0 ± 0.7
$\Delta E_{peak\text{-}area\ ratios}$ (k_BT)	-	1.7 ± 0.7	-	-

*values taken from previous study of $(H3.1\text{-}H4)_2$ tetrasomes[48],
**values taken from previous study of $(H3.3\text{-}H4)_2$ tetrasomes[49]

Supplementary Material

Modification of the Histone Tetramer at the H3-H3 Interface Impacts Tetrasome Conformations and Dynamics

Orkide Ordu[1], Leopold Kremser[2], Alexandra Lusser[3], and Nynke H. Dekker[1,*]

[1]Bionanoscience Department, Kavli Institute of Nanoscience, Delft University of Technology, Van der Maasweg 9, 2629 HZ Delft, The Netherlands
[2]Division of Clinical Biochemistry, Biocenter, Medical University of Innsbruck, Innrain 80, 6020 Innsbruck, Austria
[3]Division of Molecular Biology, Biocenter, Medical University of Innsbruck, Innrain 80-82, 6020 Innsbruck, Austria

*To whom correspondence should be addressed. Tel: +31(0)152783219; Fax: +31(0)152781202; Email: N.H.Dekker@tudelft.nl

Contents

SUPPLEMENTARY MATERIALS AND METHODS

Mass Spectrometry Experiments with IA-treated Histones

Protein bands were excised from SDS-PAGE gels and digested with trypsin from porcine pancreas (Sigma-Aldrich) as previously described in (1). Tryptic digests were analyzed using an UltiMate 3000 nano-HPLC system (Thermo Scientific by Thermo Fisher Scientific, Waltham, MA, United States) coupled to a Q Exactive HF mass spectrometer (Thermo Scientific) equipped with a Nanospray Flex ionization source. The peptides were separated on a homemade fritless fused-silica microcapillary column (75 µm i.d. x 280 µm o.d. x 10 cm length) packed with 3 µm reversed-phase C18 material (Reprosil, Ammerbuch-Entringen, Germany). Solvents for HPLC were 0.1% formic acid (solvent A) and 0.1% formic acid in 85% acetonitrile (solvent B). The gradient profile was as follows: 0-2 min, 4% B; 2-55 min, 4-50% B; 55-60 min, 50-100% B, and 60-65 min, 100 % B. The flow rate was 250 nl/min.
The Q Exactive HF mass spectrometer was operated in the data dependent mode by selecting the top 20 most abundant isotope patterns with charge >1 from the survey scan with an isolation window of 1.6 mass-to-charge ratio (m/z). Survey full scan MS spectra were acquired from 300 to 1750 m/z at a resolution of 60,000 with a maximum injection time (IT) of 120 ms, and automatic gain control (AGC) target 1e6. The selected isotope patterns were fragmented by higher-energy collisional dissociation (HCD) with a normalized collision energy of 28 at a resolution of 15,000 with a maximum IT of 120 ms, and AGC target 5e5.
Data analysis was performed using Proteome Discoverer 1.4.1.14 (Thermo Scientific) with the search engine Sequest. The raw files were searched against the *Drosophila melanogaster* database extracted from the Uniprot database. Precursor and fragment mass tolerances were set to 10 ppm and 0.02 Da, respectively, and up to two missed cleavages were allowed. Carbamidomethylation of cysteine and oxidation of methionine were set as variable modifications. Peptide identifications were filtered at 1% false discovery rate. Quantification of modified and unmodified H3.1 and H3.3 peptides was performed by summing over the respective areas under the curve (AUC) (**Fig. S2(c),(d)** below). The underlying HPLC chromatograms and MS2-spectra are shown in **Fig. S3** and **Fig. S4** below, respectively.

Salt-Dialysis Reconstitution of Tetrasomes

For the reconstitution of untreated tetrasomes, either 0.2 micrograms (µg), 0.3 µg or 0.4 µg H3.3-H4 histones were mixed with 700 nanograms (ng) of the 3.25 kbp linear DNA construct. Either 0.125 µg, 0.15 µg or 0.175 µg iodoacetamide(IA)-treated H3.3-H4 ($H3.3_{IA}$-H4) histones were mixed with 700 ng DNA for the assembly of IA-treated tetrasomes. The samples were prepared in 50 microliters (µl) high-salt buffer containing 2 molar (M) NaCl (J.T. Baker, Phillipsburg, NJ, United States), 10 millimolar (mM) Tris(hydroxymethyl)amino-methane-HCl (Tris-HCl, pH 7.4; Sigma-Aldrich, St. Louis, MO, United States), 1 mM EDTA (Sigma-Aldrich), and 1 mM DTT (Sigma-Aldrich).
Tetrasome assembly was then induced by dialyzing the samples placed in 200 ml high-salt buffer against 920 ml of a buffer containing 10 mM Tris-HCl, 1 mM EDTA, and 1 mM DTT using a multi-channel peristaltic pump (ISMATEC by Cole-Parmer, Wertheim, Germany) at a flow rate of 800 µl/min over 19 hours (h) at 4 °C. The resulting products were checked by electrophoresis on a pre-run 0.7%-agarose gel loaded with 70 ng or 140 ng sample and run in 0.1x Tris-Borate-EDTA buffer (TBE; Promega) at 80 V for 3 h at RT. The samples on the gel

were visualized by post-staining with Ethidium Bromide (Promega) for 30 min and imaged using a gel imager (ChemiDoc MP, Bio-Rad, Hercules, CA, United States) (**Fig. S5(a)** below).
The best products of each reconstitution reaction were also diluted to concentrations resembling the conditions in single-molecule experiments and analyzed by native gel electrophoresis to determine the effects of high dilutions. For this purpose, the pre-run 0.7% agarose gel was loaded with 0.4 ng of bare DNA and either 0.14 ng, 0.28 ng, or 0.56 ng of each of the two samples and run at 80 V for 3 h at RT. DNA was visualized by Sybr Gold (Invitrogen by Thermo Fisher Scientific) staining for 30 min on the gel imaged using a variable mode laser scanning imager (Typhoon TRIO, GE Healthcare, Chicago, IL, United States). The image was taken using the basic settings with the filter 488/520 BP 40 and +3 mm focal depth, and the variable settings set to high sensitivity at 550 PMT with a pixel size of 100 µm (**Fig. S5(b)** below).

Flow Cell Assembly and Preparation for Single-molecule Experiments

The lower coverglass was coated with 2.5 ul of a 0.1% solution of nitrocellulose (Invitrogen) dissolved in pentyl acetate solution (Sigma Aldrich). One flow cell was used for each experiment. The flow cell was prepared by first incubating for 1 h with 100 µl of amine-coated polystyrene beads (1 µm diameter, Polysciences, Warrington, PA, United States) diluted by 1:2500 or 1:5000 in a buffer containing 100 mM NaCl, 10 mM Tris-HCl, and 1 mM EDTA (TE buffer). Unbound beads were then washed out with 300-500 µl TE buffer. Subsequently, the flow cell was put on a heat-plate for 100-120 s at 100 °C to melt down the bound polystyrene beads for stable adhesion to the nitrocellulose-coated surface. After subsequent rinsing with 300-500 µl buffer, the flow cell was washed and incubated overnight with 100 µl of a 0.1 mg/ml solution of anti-digoxigenin antibody fragments (Roche) dissolved in PBS (Sigma-Aldrich). The next day, the flow cell was washed with 300-500 µl TE buffer and passivated with 100 µl of a 20 mg/ml Bovine Serum Albumin (BSA) solution (New England Biolabs, Ipswich, MA, United States) diluted 1:1 in TE buffer.
Thus functionalized, the flow cell was then prepared for tethering of DNA constructs by washing with 500-1000 µl TE buffer containing 0.015% Triton-X (Sigma-Aldrich; TE-TX buffer). 0.2 or 0.4 µl of a solution with superparamagnetic beads (0.5 µm diameter, Ademtech, Pessac, France) were washed three times in 10 µl of TE-TX buffer, then mixed and incubated for 10 min with 0.4 or 0.8 µl of a DNA solution diluted 1:100 from the stock solution with a DNA concentration of 16 ng/µl. Upon a subsequent dilution by 1:100, 100 µl of the DNA/bead solution was flushed into the flow cell and incubated for 2-3 h for tethering to the functionalized coverglass. Unbound tethers were flushed out with at least 2 ml buffer for a clean flow cell to start the experiment.

Magnetic Tweezers Hardware

The hardware of the magnetic tweezers setup used in this study has been detailed previously (2). In brief, the flow cell containing the sample is illuminated from the top by a light-emitting diode (LED; Lumitronix, Hechingen, Germany). The transmitted light is collected by a 100x oil-immersion objective (Olympus, Tokyo, Japan) and directed onto a complementary metal-oxide semiconductor (CMOS) camera (Teledyne Dalsa, Waterloo, Canada) operated at an acquisition rate of 100 Hz. By this means of video microscopy, the bead's position is tracked with nanometer accuracy using a custom-written tracker software

(3). In this FOMT-based study, the bead is subject to a magnetic field generated by a cylindrical permanent magnet stacked of three ring-shaped magnets (Supermagnete, Gottmadingen, Germany) and positioned between the flow cell and the LED. The DNA tethers were aligned with the magnet axis by manually and/or electronically positioning the custom-built sample stage using linear actuators of sub-micrometer precision (Physik Instrumente, Karlsruhe, Germany).

Data Analysis

The recorded, raw time traces of the bead's lateral position in *x*, *y*, and vertical position in *z* were converted into the corresponding time traces of the linking number and the length of the tethered DNA molecule, respectively, as described in (4). The time windows in which proteins were flushed in, and so the bead was subject to fluid flow, were cut out before the subsequent quantitative analysis of the traces, which was performed as briefly described in **Materials and Methods** in the main text**.**

In the determination of the steps coinciding in both time traces, a maximum time difference of 18.4 s, deduced from autocorrelation analysis of the bead's rotational fluctuations (**Fig. S6** below), was tolerated between the steps. By this means, 43% (*n*=33) of all identified coinciding steps (*N*=76) were detected automatically, while 63% (*n*=48) were determined after manually correcting misidentified steps to better match the data.

The sizes of all thus determined steps were further compared against the mean spatial resolution, essentially corresponding to the experimental measurement error. The time traces contain intrinsic time-correlated fluctuations that result from the (dominant) thermal motion of the tethered beads and hardware-inherent noise. These values supported a more reliable interpretation of the fitted steps, as those with sizes below the mean spatial resolution might also be the result of experimental drift or artifacts by the step-fitting algorithm due to the high noise in the time traces. Therefore, steps coinciding in both time traces of individual measurements were considered to have been induced by tetrasome assembly, regardless of their size. The mean spatial resolution was calculated for both quantities by averaging over the standard deviations (STDs) from the functions fitted to their time trace profiles. In general, the length data was fitted by a gamma function after mirroring at the x-axis to compensate for the slight skew of the data towards smaller values, possibly due to attractive bead-surface interactions. As the spatial resolution in one experiment, the average of the STDs from gamma fits to three (in one case two) different parts of the longest durations between two subsequent steps were considered. The linking number data was fitted to a corresponding number of Gaussian functions. Here, the spatial resolution in one experiment was determined by the STD from the fit of a single Gaussian function to the data in the initial part of the time trace, before proteins were flushed in.

In the employed dwell time analysis for a more detailed picture of the handedness dynamics, the traces were filtered by averaging over either a number *N*=340 or *N*=1840 data points which, based on the acquisition rate of 100 Hz, correspond to a time average of 3.4 s or 18.4 s, respectively, in agreement with the results from the autocorrelation analysis of the bead's rotational fluctuations (**Fig. S6** below). This approach ensured the decoupling of the beads' thermal motion from the flipping dynamics of the tetrasomes. The extent of the filtering

proved to be very critical due to its high impact on the overall results such that no preference could be made between the two approaches for an explicit statement about the total dwell times. By extending the threshold into a zone, only linking number changes upon flipping that were greater than this threshold zone were considered, while mostly events in the noisy, undefined region at the overlap of the two states were disregarded by adding their dwell times to that in the current state up to that point. Likewise, detected events with dwell times shorter than the mean characteristic time of the bead's rotational fluctuations (bead response time) of 3.4 s (**Fig. S6** below) were corrected for in a last step.

In the separate analysis of the recorded dwell times in the plateaus of the steps fitted by the step-fitting algorithm, some of the flipping events were missed and steps introduced which do not match the data very well, although the algorithm was allowed to overfit to detect as many states as possible (**Fig. 4(b)** in main text). Such steps were manually corrected for a better match to the data and a more reliable dwell time analysis. The mean dwell times were determined by an exponential fit to the combined data sets assigned to the left-handed (*N*=65) and right-handed state (*N*=64) and, if applicable, cut off at the mean dissocation time reduced by 1 standard error of the mean (SEM; **Fig. S7** below), i.e. 2084 s.

In the re-analysis of the partial traces from an earlier experiment with untreated $(H3.1\text{-}H4)_2$ tetrasomes presented in (5), the resulting mean dwell time for the left-handed state was multiplied by a factor of three to obtain the life time for a single left-handed tetrasome, as three independent tetrasomes were assembled on the DNA molecule here. Since a second tetrasome only flipped with relative occurrences of 2.7% and 0.7% in two of the partial time traces, all data assigned to the right-handed state was considered as flipping events of one tetrasome.

SUPPLEMENTARY TABLES

Table SI. The sequences of the primers used to generate the DNA constructs. Lowercases indicate the specific overhangs at the BsaI sites.

Primers	Primer Sequences
1	5'-CTGCGGTCTCGtaggCCTCAGCGACGCAGGGGACCTGCAGG
2	5'-CTGCGGTCTCGtcaaTGCCGTTGTAACCGGTCATC
3	5'-CCATCTTGGTCTCCcctaCGCTCTAGAACTAGTGGATCCCCC
4	5'-CCATCTTGGTCTCCttgaCGCTCTAGAACTAGTGGATCCCCC
5	5'-GACCGAGATAGGGTTGAGTG

SUPPLEMENTARY FIGURES

(a)

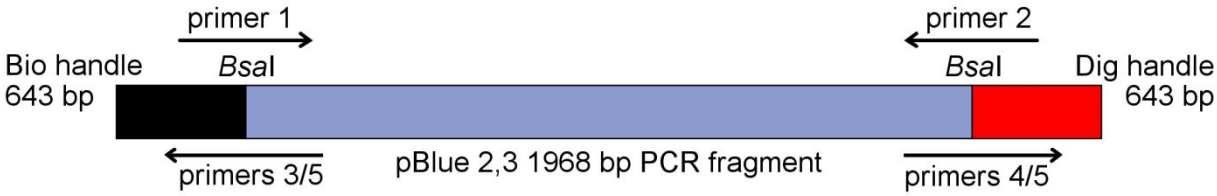

(b)

CTGCGGTCTCGtcaaTGCCGTTGTAACCGGTCATCCCCGAGTACGGCTGCAGCGCCCGCGTCCG
GCTGACCAGCGTGCCGGACACCGGCAGCACGGCGATGCCGTTCATGACCTGATAACTGCGGG
CCTGTCGTGGTCCGTCATCATCACCGGATAATGCCAGCGTCGCGAGTGCCTCCTGGGCAGTCA
GGCTGTCGCCGGACACCGCATCCGTCAGGCTGCTGATCCCAAGCTGGCCTGCAAGCGCACAAA
AGAAAACCCGCGCATAGGCGGGTTCAAGCATCAGCGGCTCATTAAAGGCCATGCTGGCAATATG
CGGGAGATTACGCAGCTCTGCTGTCACTCTTCTCCTCCTCTGTTGATTGTCGCAGCCCGGATTC
AAATGCTGCAGCCGCCCAGGCGGGCGGTTTAAGACCGGCTGCACGGCGCTCCATCGTTTCACG
GACCTGCTGGGCAAAAATTTCCTGATAGTCGTCACCGCGTTTTGCGCACTCTTTCTCGTAGGTAC
TCAGTCCGGCTTCTATCAGCATCACCGCTTCCTGAACTTCTTTCAGACCATCGATGGCCATACGA
CCGGAGCCTATCCAGTCGCAGTTCCCCCAGGCACTGCGGGCTTCCTGAAAACTGAAGCGCGCT
TTTGAAGGTAACGTCACCACGCGGCGAACGATGGCCTCTTCCAGCCAGCACAGAAACATCTGGC
TCGCCTGACGGGATGCGACGAATTTTCGCCGCCCCATAAAGTACGCCCACGACTCGTTCGCACT
GGCCCGTGCCGTGGAGTAGCTCATCTGGGCGTAATTCCGGGAAAGCTGCTCATACGAGACACC
CAGCCCGGCAGCGATATACCGCAGCAGTGACTGCTCAAACACGGAGTAGCCGTTATCCGTATC
CTGAGCCGTCTGCAGGTTCAGTGAGTCACCCGGCATCAGGTGCGGTACTTTTGCGCCTCCCAG
CCGGACCGGCGCTGCGGCGTAATACGCGGCAATTTCACCAATCCAGCCGGTCAGCCTTTCCCG
CTGCTCCTGACTGTTCGCGCCCAGAATAAAATCCATCGCTGACTGCGTATCCAGCTCACTCTCAA
TGGTGGCGGCATACATCGCCTTCACAATGGCGCTCTGCAGCTGCGTGTTCTGCAGCGTGTCGA
GCATCTTCATCTGCTCCATCACGCTGTAAAACACATTTGCACCGCGAGTCTGCCCGTCCTCCAC
GGGTTCAAAAACGTGAATGAACGAGGCGCGCCCGCCGGGTAACTCACGGGGTATCCATGTCCA
TTTCTGCGGCATCCAGCCAGGATACCCGTCCTCGCTGACGTAATATCCCAGCGCCGCACCGCTG
TCATTAATCTGCACACCGGCACGGCAGTTCCGGCTGTCGCCGGTATTGTTCGGGTTGCTGATGC
GCTTCGGGCTGACCATCCGGAACTGTGTCCGGAAAAGCCGCGACGAACTGGTATCCCAGGTGG
CCTGAACGAACAGTTCACCGTTAAAGGCGTGCATGGCCACACCTTCCCGAATCATCATGGTAAA
CGTGCGTTTTCGCTCAACGTCAATGCAGCAGCAGTCATCCTCGGCAAACTCTTTCCATGCCGCTT
CAACCTCGCGGGAAAAGGCACGGGCTTCTTCCTCCCCGATGCCCAGATAGCGCCAGCTTGGGC
GATGACTGAGCCGGAAAAAAGACCCGACGATATGATCCTGATGCAGCTGGATGGCGTTGGCGG
CATAGCCGTTATTGCGTACCAGATCGTCTGCGCGGGCATTGCCACGGGTAAAGTTGGGCAACA
GGGCTGCATCCACACTTTCACTCGGTGGGTTCCACGACCGCAACTGCCCTCCAAATCCGCTGCC
ACCGCCGTGATAACCGGCATATTCGCGCAGCGATGTCATGCCGTCCGGCCCCAGAAGGGTGGG
AATGGTGGGCGTTTTCATACATAAAATCCTGCAGGTCCCCTGCGTCGCTGAGGcctaCGAGACCG
CAG

FIG. S1. Details of the DNA construct used in this study. (a) Schematic depiction of the 1.97 kbp linear DNA fragment (light purple) generated from a pBluescript (pBlue) 2,3 plasmid by Polymerase Chain Reaction (PCR) with primers 1 and 2. Shorter, either biotin- (Bio, black) or digoxigenin-coated (Dig, red) fragments (handles) of 643 bp generated by primers 3 and 4, respectively, in combination with primer 5, were each ligated via BsaI sites to either end. For details on the preparation of the DNA constructs, see **Materials and Methods** in main text and **Table SI** above. **(b)** Sequence of the main DNA segment.

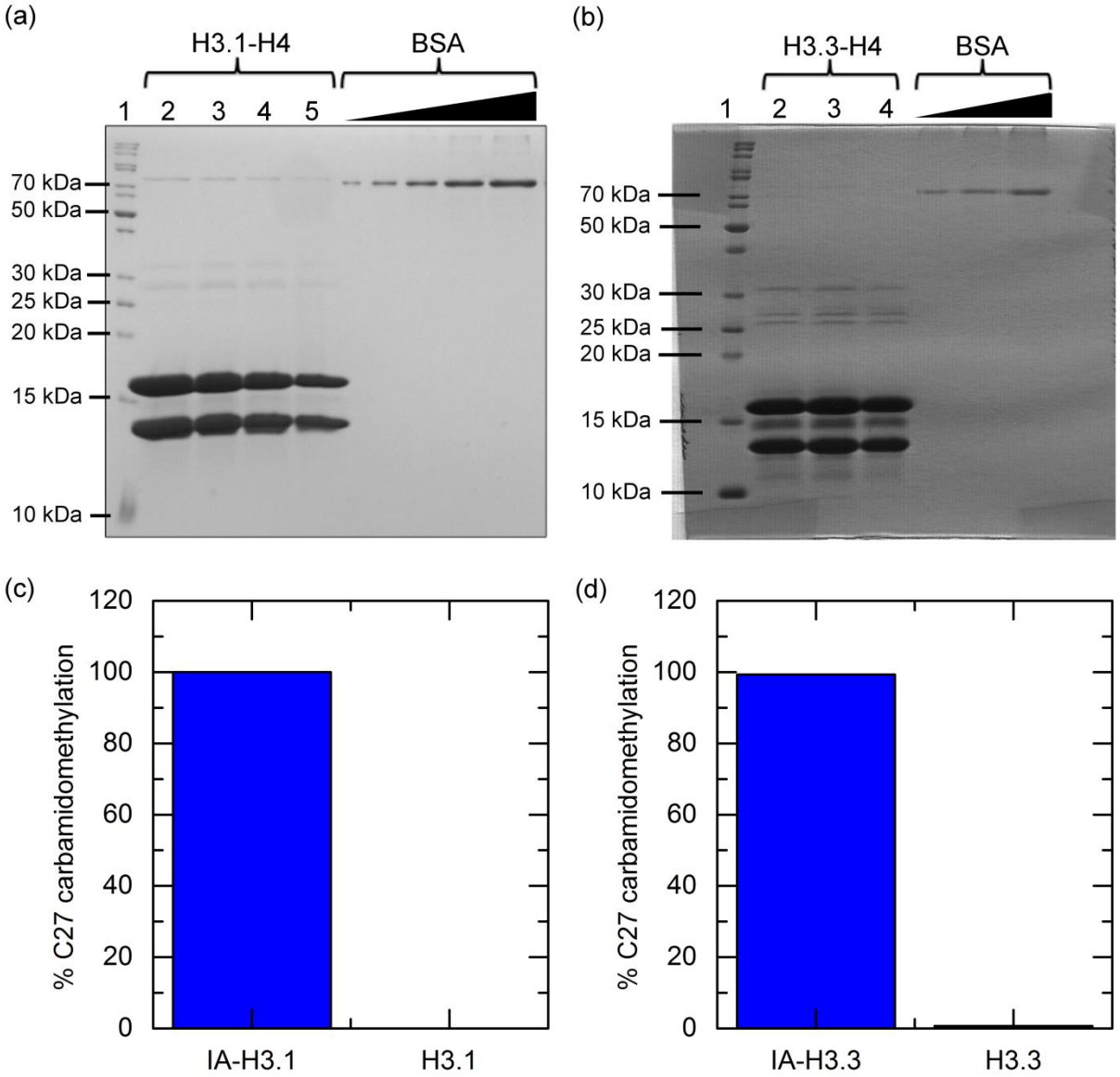

FIG. S2. Purified and IA-treated histones. (a), (b) Protein gels stained with Coomassie blue showing H3.1-H4 and H3.3-H4 histones, respectively, before (lanes 2) and after dialysis into a buffer suitable for the IA-treatment (lanes 3), as well as after the treatment (lane 4 in (a), not shown in (b)) and after another dialysis to remove IA (lane 5 in (A), lane 4 in (b)). The total concentrations of histones in the equimolar samples were estimated to 2 µg/µl and 280 ng/µl, respectively, from BSA standards (subsequent lanes with 50 ng, 100 ng, 200 ng, 400 ng, 600 ng in (a), and 100 ng, 200 ng, 400 ng in (b)). **(c)**, **(d)** Mass spectrometry analysis of IA-treated histones H3.1 ($H3.1_{IA}$) and H3.3 ($H3.3_{IA}$), respectively, showing complete (100%, (c)) or near complete ((d), 99.3%) conversion of the cysteine residues into carbamidomethyl-cysteine. Values were calculated from the sum of the respective areas under the curve (AUC) of C27-containing peptides with or without carbamidomethylation.

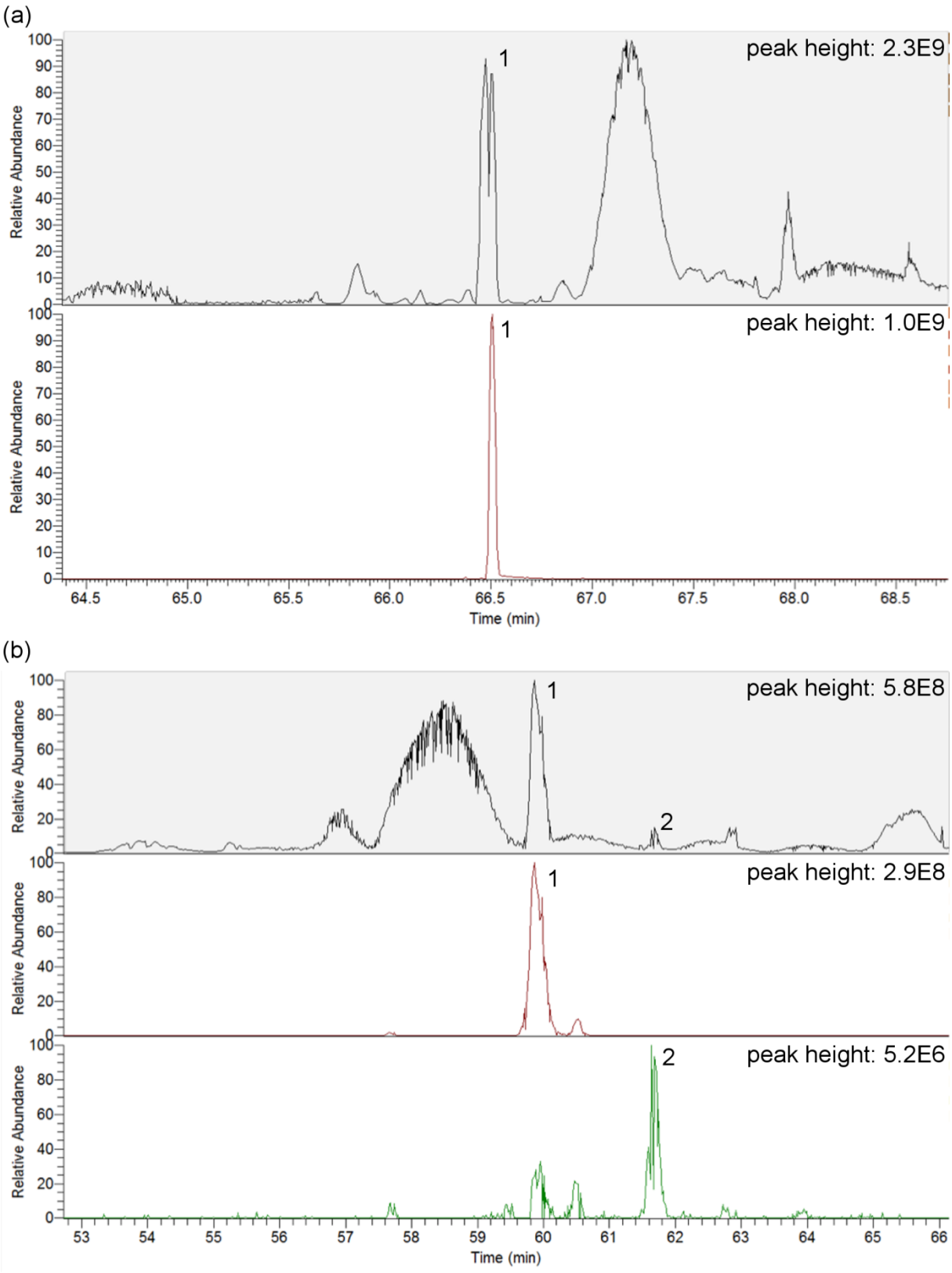

FIG. S3. HPLC chromatograms. **(a)** Base peak (top) and extracted ion chromatogram (bottom) of H3.1 digest. Only the carbamidomethylated peptide spanning amino acids 85-116 (peak 1) was found. **(b)** Base peak (top) and extracted ion chromatograms (middle, bottom) of H3.3 digest. Peak 1 corresponds to the carbamidomethylated peptide 85-116, while peak 2 depicts the unmodified peptide.

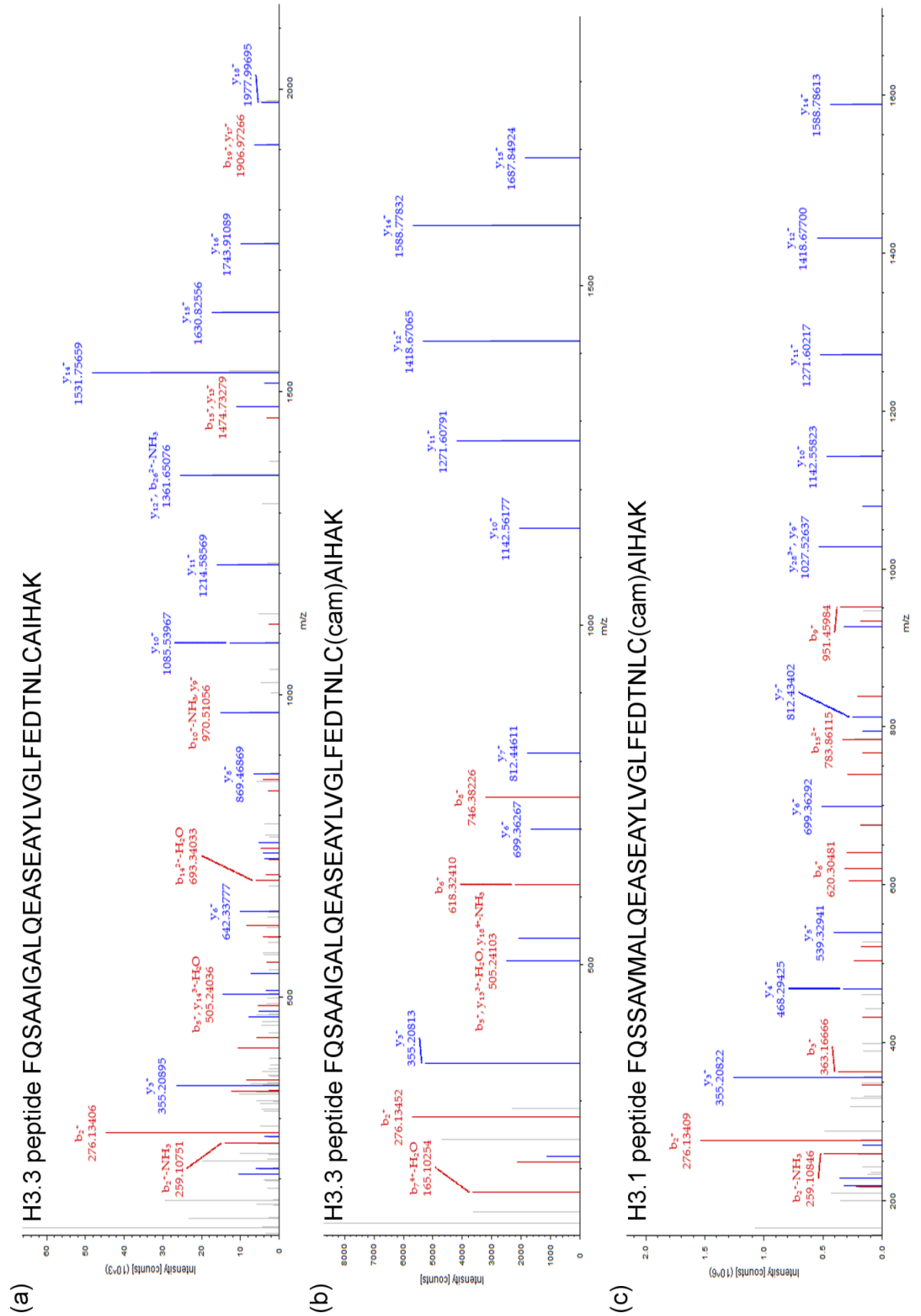

FIG. S4. MS2-spectra of the histone H3 peptides. (a), (b) MS2-spectra of the unmodified (a) and carbamidomethylated (b) histone H3.3 peptide spanning amino acids 85-116. **(c)** MS2-spectrum of the carbamidomethylated histone H3.1 peptide 85-116.

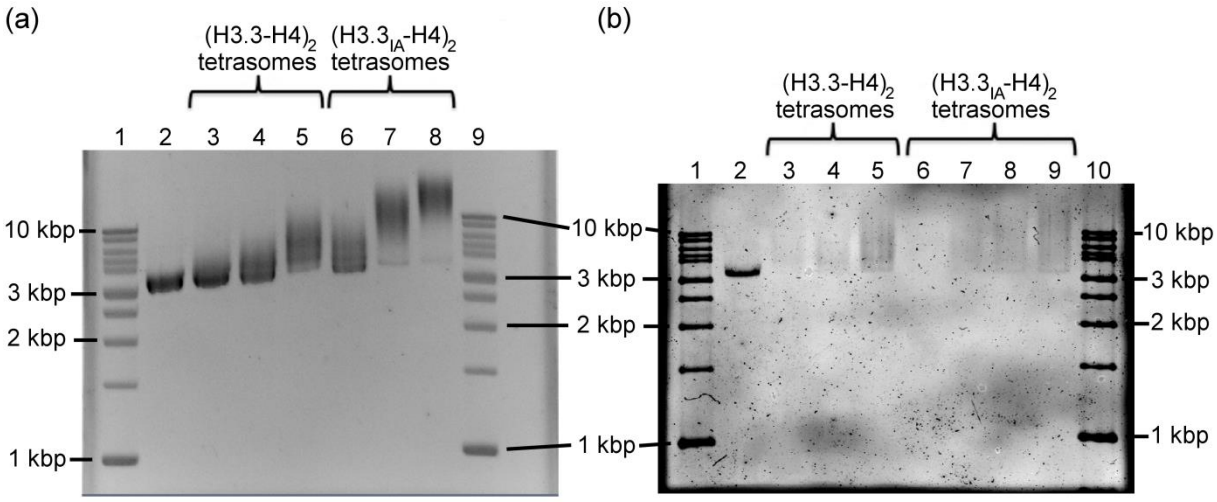

FIG. S5. Untreated and $(H3.3_{IA}\text{-}H4)_2$ tetrasomes reconstituted via salt-dialysis. (a) 0.7%-agarose gel of reconstitution products using three different concentrations of untreated (lanes 3-5) and $(H3.3_{IA}\text{-}H4)_2$ tetramers (lanes 6-8) and a 3.25 kbp long linear DNA fragment (lane 2). Increasing amounts of untreated H3.3-H4 histones (0.2 µg, 0.3 µg, 0.4 µg in lanes 3-5) or $H3.3_{IA}$-H4 histones (0.125 µg, 0.15 µg, 0.175 µg in lanes 6-8) were loaded onto 700 ng DNA. After reconstitution via salt-dialysis, 70 ng (lanes 2 and 3) or 140 ng (lanes 4-8) of DNA assembled into tetrasomes were loaded onto the gel and stained with ethidium bromide. Lanes 1 and 9 contain the DNA size marker. **(b)** 0.7%-agarose gel showing different dilutions of lanes 5 and 7 from (a) stained with Sybr Gold. The degrees of dilution (1:1000, 1:500, and 1:250 in lanes 3-5 and 7-9, respectively) correspond to conditions used in single-molecule experiments. The shift of the DNA smears towards reduced molecular weights indicates at least partial disassembly upon dilution. Lanes 1 and 10 contain the DNA size marker.

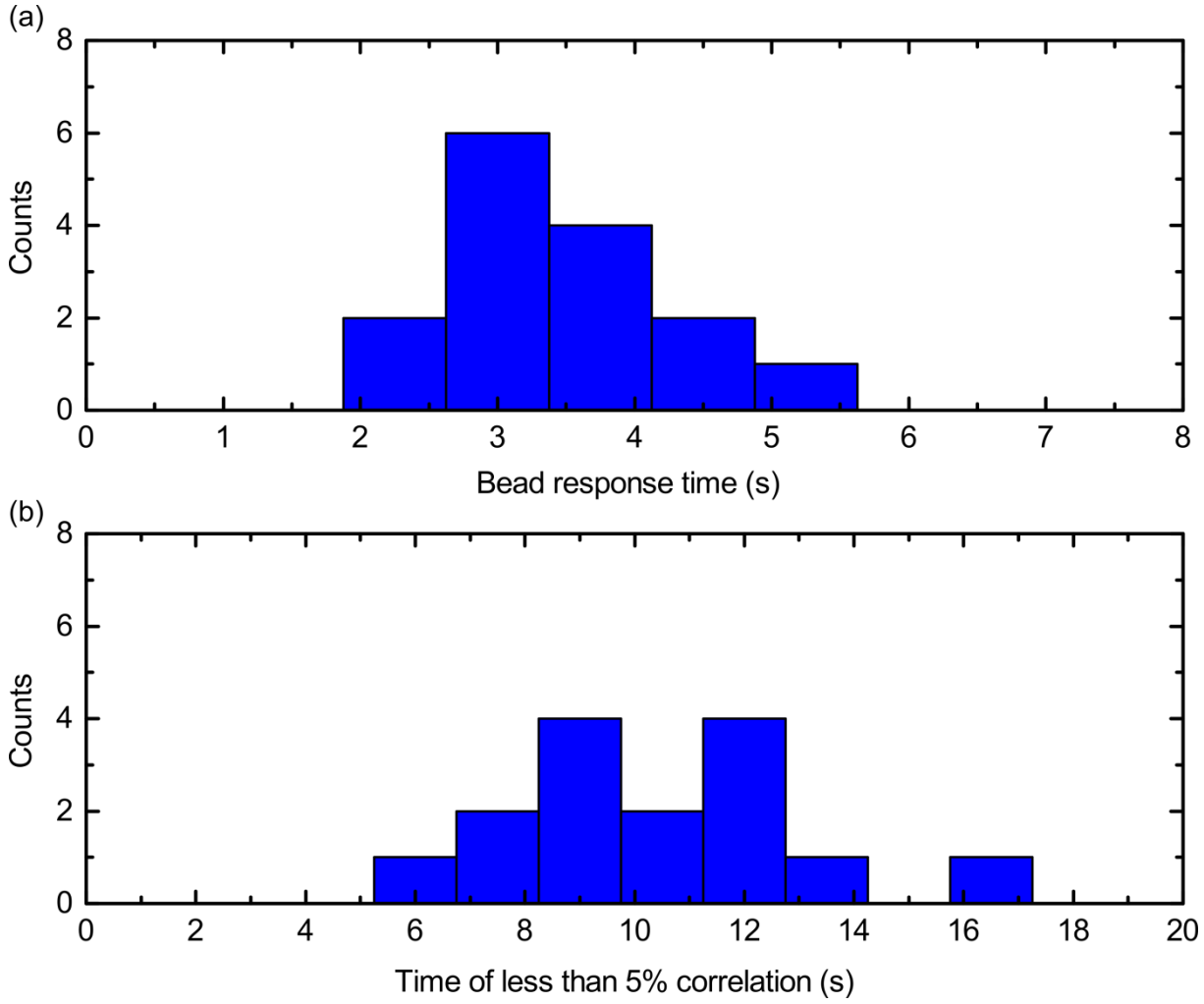

FIG. S6. Characteristic times of the measured fluctuations in the linking number of bare DNA molecules. (a) Histogram of the bead response times for a 1.97 kbp DNA segment tethered to a small paramagnetic bead (diameter of 500 nm). The response times are determined from autocorrelation analysis of the DNA linking number time traces measured in FOMT experiments (4). Knowledge of the bead's response time, characterizing its thermal motion, is critical for both the identification of coinciding steps in the time traces of DNA length and linking number upon tetrasome assembly or disassembly, and for the dwell time analysis. The data yielded a mean value of τ_c = 3.4 ± 0.9 s. **(b)** Histogram of the first times at which the autocorrelation is below 5%, showing a mean value of τ_c = 10.3 ± 2.7 s. This mean value plus three STDs (τ_c = 18.4 s) was employed as an upper cutoff for the time difference between assembly or disassembly steps in both quantities to be identified as coinciding. These values also provided the filtering time scales for the time traces subjected to dwell time analysis (see **Supplementary Materials and Methods** above).

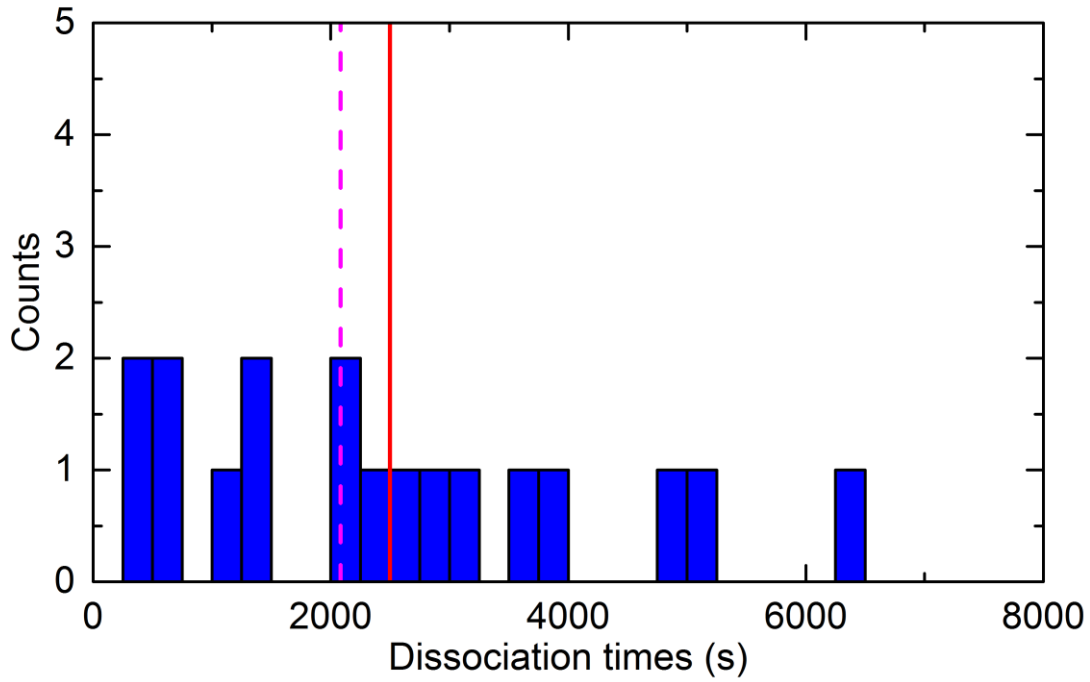

FIG. S7. Distribution of the dissociation times for ($H3.1_{IA}$-H4)$_2$ tetrasomes. IA-treated (H3.1-H4)$_2$ tetrasomes were found to disassemble at different times during the experiments. These dissociation times can be critical for the study of the dynamics, but they are distributed broadly: the mean value of 2499 s (red line) with a standard deviation (STD) of ±1763 s is poorly defined. Therefore, the mean value subtracted by 1 standard error of the mean (1 SEM = 415 s) at 2084 s (dashed magenta line) is considered, e.g. in the dwell time analysis.

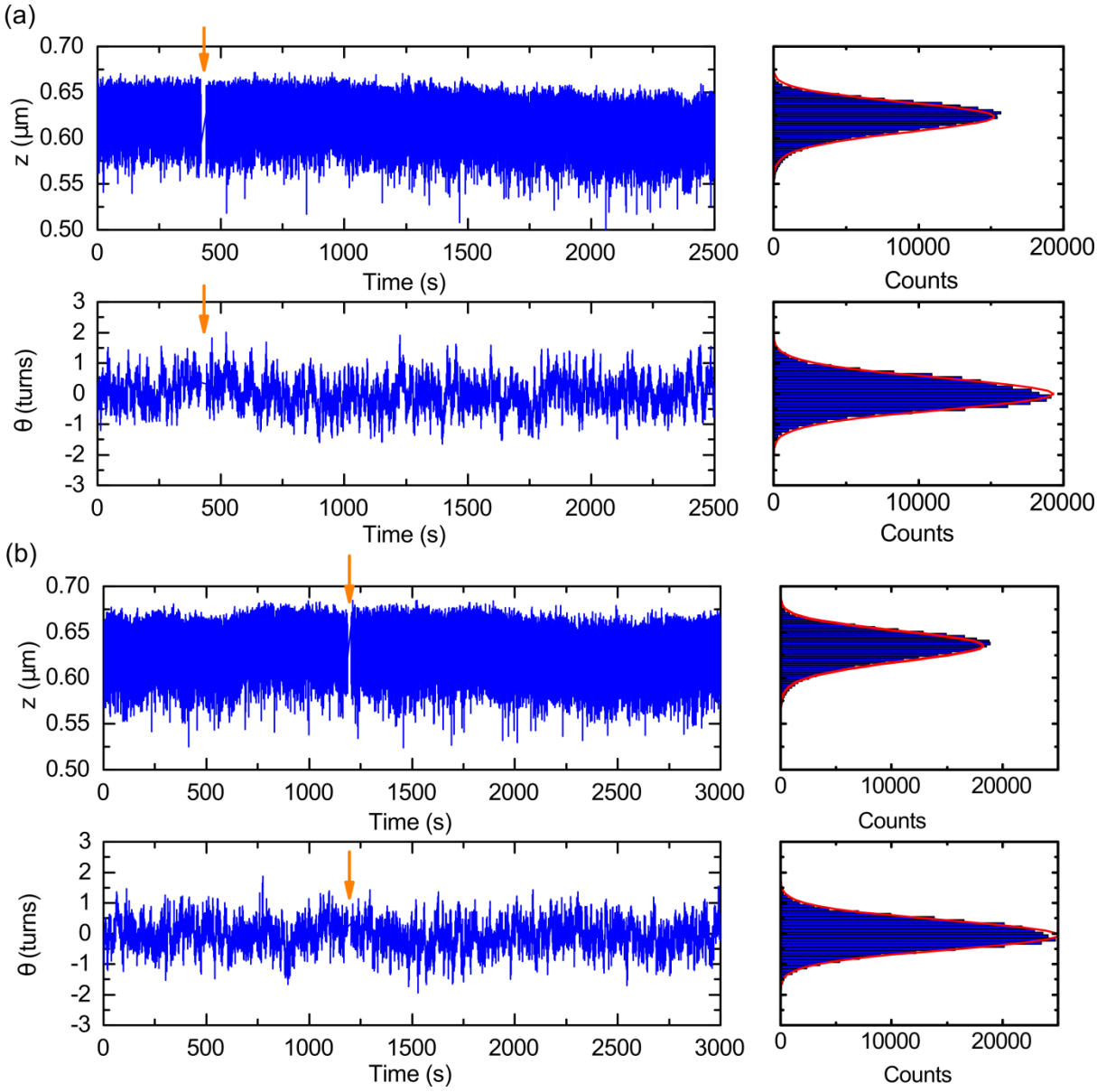

FIG. S8. Example traces with the individual proteins. (a) Time traces of length *z* (in µm, upper panel) and linking number *Θ* (in turns, lower panel) of a DNA molecule before and after flushing in (orange arrows) $(H3.1_{IA}\text{-}H4)_2$ tetramers without pre-incubation with NAP1 under the standard conditions in this study (see **Materials and Methods** in main text). As the singly peaked mirrored gamma (due to the slight skew of the data to smaller values) and normal distributions (red) indicate, the histone tetramers do not assemble into tetrasomes in the absence of NAP1. **(b)** Time traces of DNA length *z* (upper panel) and linking number *Θ* (lower panel) of a DNA molecule before and after flushing in (orange arrows) only NAP1 proteins under the standard conditions in this study. As the singly peaked mirrored gamma (due to the slight skew of the data to smaller values) and normal distributions (red) indicate, NAP1 alone does not interact with the DNA molecule.

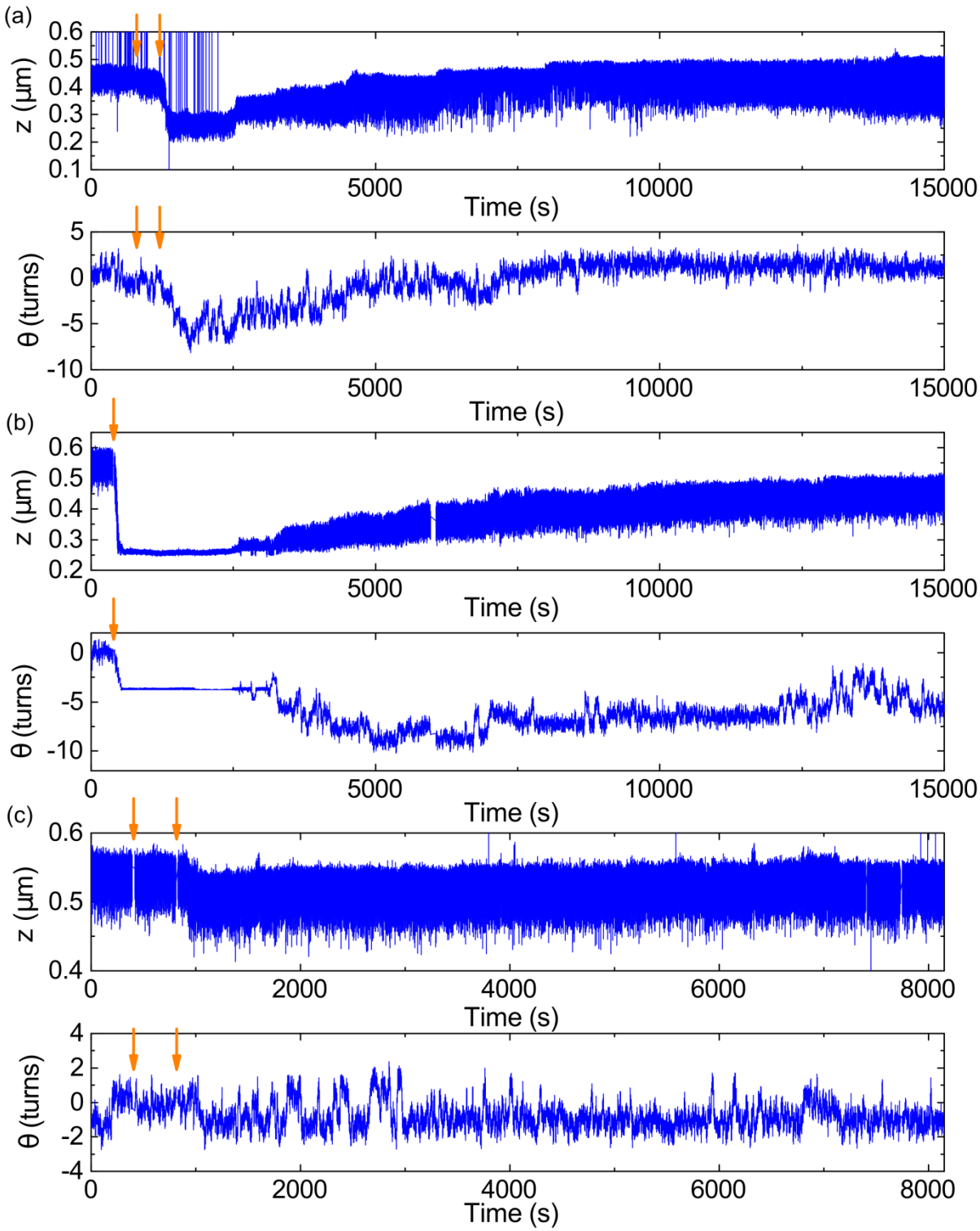

FIG. S9. Example traces with different ratios of IA-treated histones and NAP1. (a) Time traces of length z (in µm, upper panel) and linking number Θ (in turns, lower panel) of an initially bare DNA molecule with $(H3.3_{IA}\text{-}H4)_2$ tetrasomes assembled after flushing in (orange arrows) 108 nM $H3.3_{IA}$-H4 histones pre-incubated with 192 nM NAP1, i.e. in a ratio of 1:1.8. Initially (up to about 2000 s), the z position is not very well tracked, which results in some spikes, but does not affect the overall signal. As indicated by the stepwise increases in DNA

length and linking number, the modified tetrasomes also disassembled under these conditions. **(b)** Time traces of DNA length *z* and linking number *Θ* of an initially bare DNA molecule with $(H3.3_{IA}\text{-}H4)_2$ tetrasomes assembled after flushing in (orange arrows) 127 nM $H3.3_{IA}$-H4 histones incubated with 192 nM NAP1, i.e. in a ratio of 1:1.5. Here, the modified tetrasomes even disassembled from a fully assembled DNA molecule. While the assembly of the multiple tetrasomes in both (a) and (b) happened simultaneously in the form of large steps, they mainly disassembled in a one-by-one fashion, indicating the formation of proper individual complexes (see main text and **Fig. 3(b)**). **(c)** Time traces of DNA length *z* and linking number *Θ* of an initially bare DNA molecule with $(H3.1_{IA}\text{-}H4)_2$ tetrasomes after flushing in (orange arrows) 100 nM $H3.1_{IA}$-H4 histones incubated with 113 nM NAP1, i.e. in a ratio of 1:1.1. Here, the modified tetrasome did not disassemble over the total measurement time, while it exhibited the same handedness dynamics, within error, as quantified by analyzing the dwell times in the step plateaus from the step-fitting algorithm ($\tau_{D,left}$ = 326 s and $\tau_{D,right}$ = 79 s, see **Materials and Methods**, and **Table I** in main text).

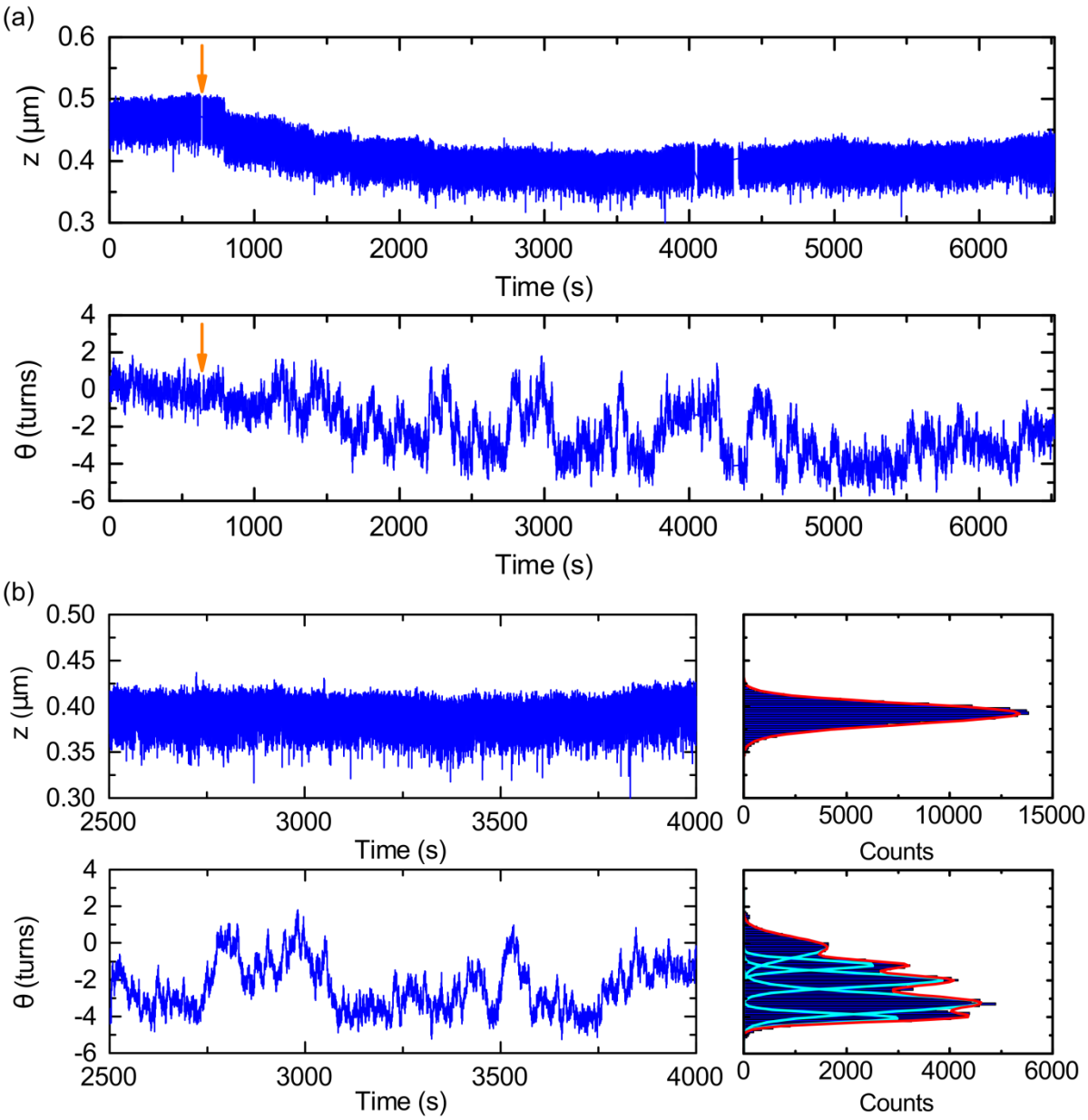

FIG. S10. Example time traces with untreated tetrasomes in the same buffer conditions as the IA-treated tetrasomes. (a) Time traces of length *z* (in μm, upper panel) and linking number *Θ* (in turns, lower panel) of an initially bare DNA molecule with $(H3.3\text{-}H4)_2$ tetrasomes assembled after flushing in (orange arrows) $(H3.3\text{-}H4)_2$ tetramers pre-incubated with NAP1 under the standard conditions in this study (see **Materials and Methods** in main text). The untreated tetrasomes do not disassemble during the experiment. **(b)** Partial time traces from (a) to illustrate the handedness dynamics of the untreated tetrasomes. While the DNA length stays constant (upper panel), the linking number *Θ* (lower panel) is observed between several discrete levels. The four assembled tetrasomes occupy five states whose populations were fit to normal distributions (individual fits in cyan; sum of all fits in red).

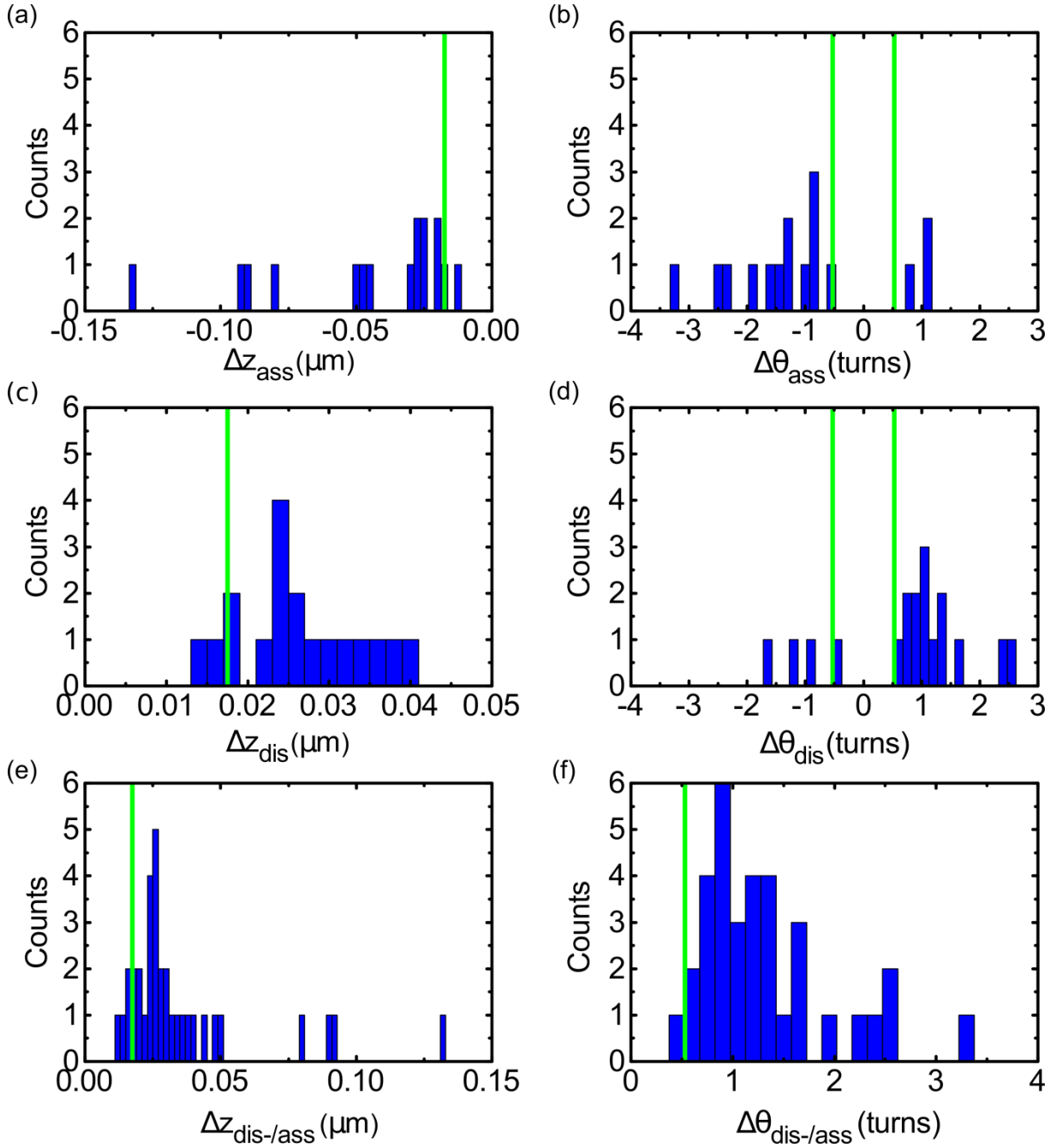

FIG. S11. Changes in DNA length and linking number upon assembly and disassembly of $(H3.1_{IA}\text{-}H4)_2$ tetrasomes. (a) Histogram of changes in DNA length Δz (in µm) upon assembly, **(c)** upon disassembly, and **(e)** upon both assembly and disassembly of $(H3.1_{IA}\text{-}H4)_2$ tetrasomes. The mean spatial resolution based on 1 standard deviation (1 STD = 18 nm) is indicated by the green line. **(b)** Histogram of changes in DNA linking number $\Delta\Theta$ upon assembly, **(d)** upon disassembly, and **(f)** both upon assembly and disassembly of $(H3.1_{IA}\text{-}H4)_2$ tetrasomes. The mean spatial resolution based on 1 STD (0.5 turns) is indicated by the green line. The absolute values of the combined data (panels (e) and (f), N=34) yielded mean values of $\Delta z_{dis-/ass}$ = 29 ± 8 nm (n=24) and $\Delta\Theta_{dis-/ass}$ = 1.1 ± 0.3 turns (n=27) obtained from the data within the range bounded by the resolution limit (green lines) and the DNA contour length wrapped in a full nucleosome (50 nm) and the number of turns it is wrapped around the histone core (1.7 turns), respectively.

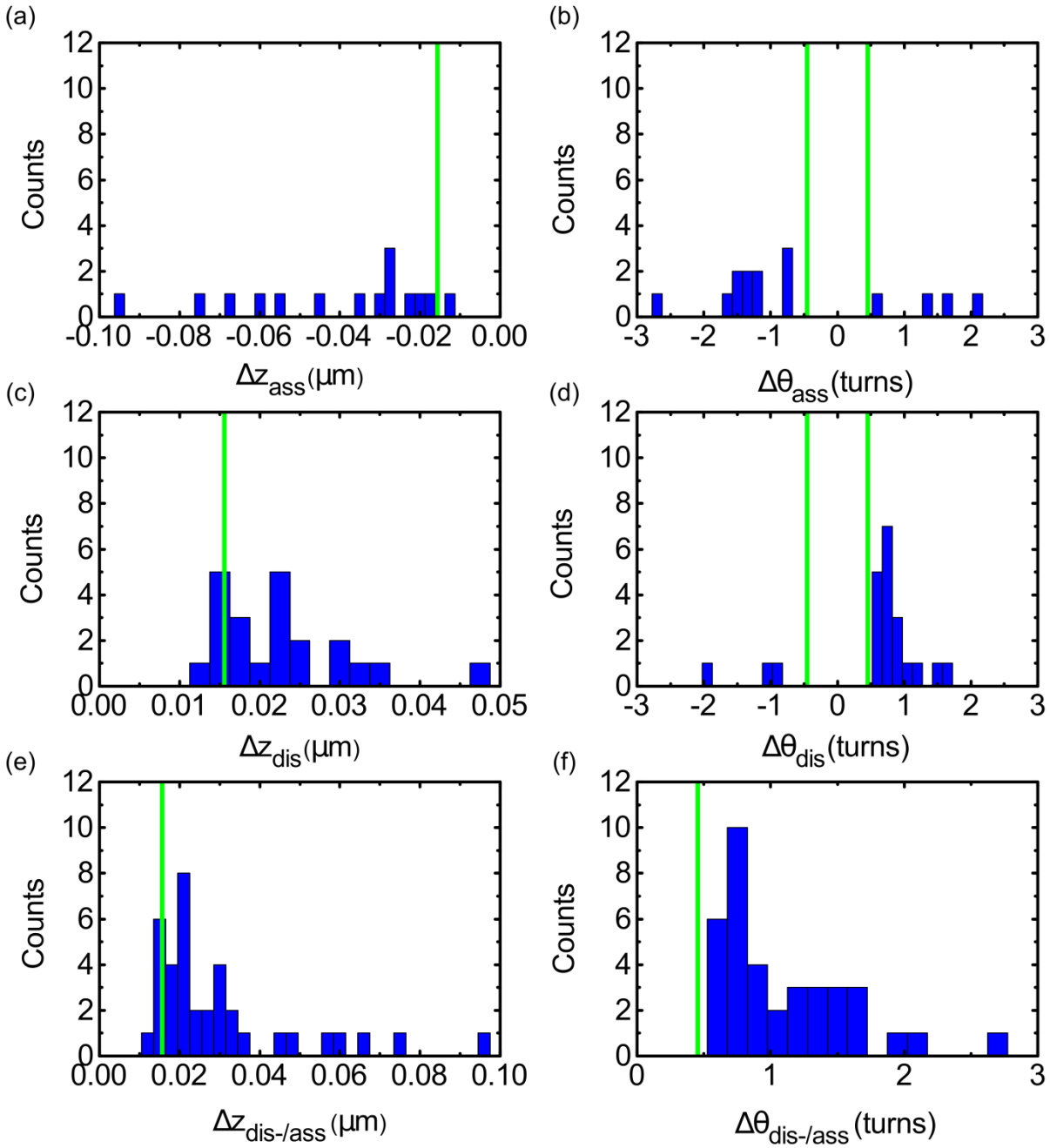

FIG. S12. Changes in DNA length and linking number upon assembly and disassembly of $(H3.3_{IA}\text{-}H4)_2$ tetrasomes. (a) Histogram of the changes in DNA length Δz (in μm) upon assembly, **(c)** upon disassembly, and **(e)** both assembly and disassembly of $(H3.3_{IA}\text{-}H4)_2$ tetrasomes. The mean spatial resolution based on 1 STD (16 nm) is indicated by the green line. **(b)** Histogram of changes in DNA linking number $\Delta\Theta$ (in turns) upon assembly, **(d)** upon disassembly, and **(f)** both assembly and disassembly of $(H3.3_{IA}\text{-}H4)_2$ tetrasomes. The mean spatial resolution based on 1 STD (0.5 turns) is indicated by the green line. The absolute values of the combined data (panels (e) and (f), N=37) yielded mean values of $\Delta z_{dis\text{-}/ass}$ = 26 ± 8 nm (n=27) and $\Delta\Theta_{dis\text{-}/ass}$ = 1.0 ± 0.3 turns (n=34) obtained from the data within the range bounded by the resolution limit (green lines) and the DNA contour length wrapped in a full nucleosome (50 nm) and the number of turns it is wrapped around the histone core (1.7 turns), respectively.

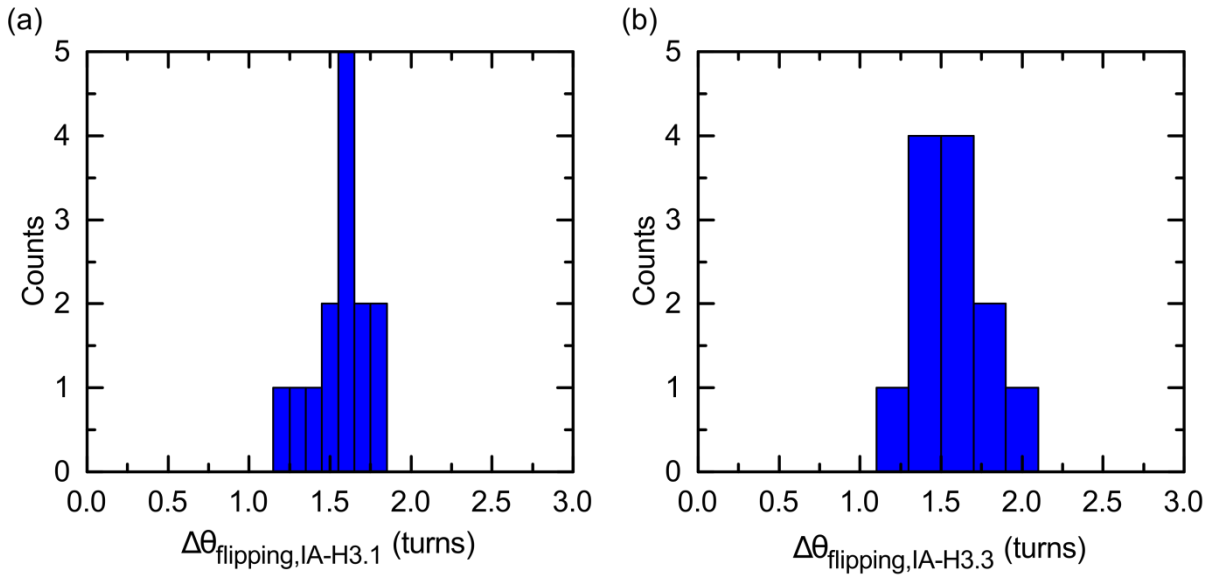

FIG. S13. Change in linking number upon handedness flipping of IA-treated tetrasomes. (a) Histogram of the changes in linking number $\Delta\Theta_{flipping}$ (in turns) upon the handedness flipping of $(H3.1_{IA}\text{-}H4)_2$ tetrasomes. The data has a value of $\Delta\Theta_{flipping}$ = 1.6 ± 0.2 turns. **(b)** Histogram of the changes in linking number upon the handedness flipping of $(H3.3_{IA}\text{-}H4)_2$ tetrasomes. The data has a mean value of $\Delta\Theta_{flipping}$ = 1.6 ± 0.2 turns.

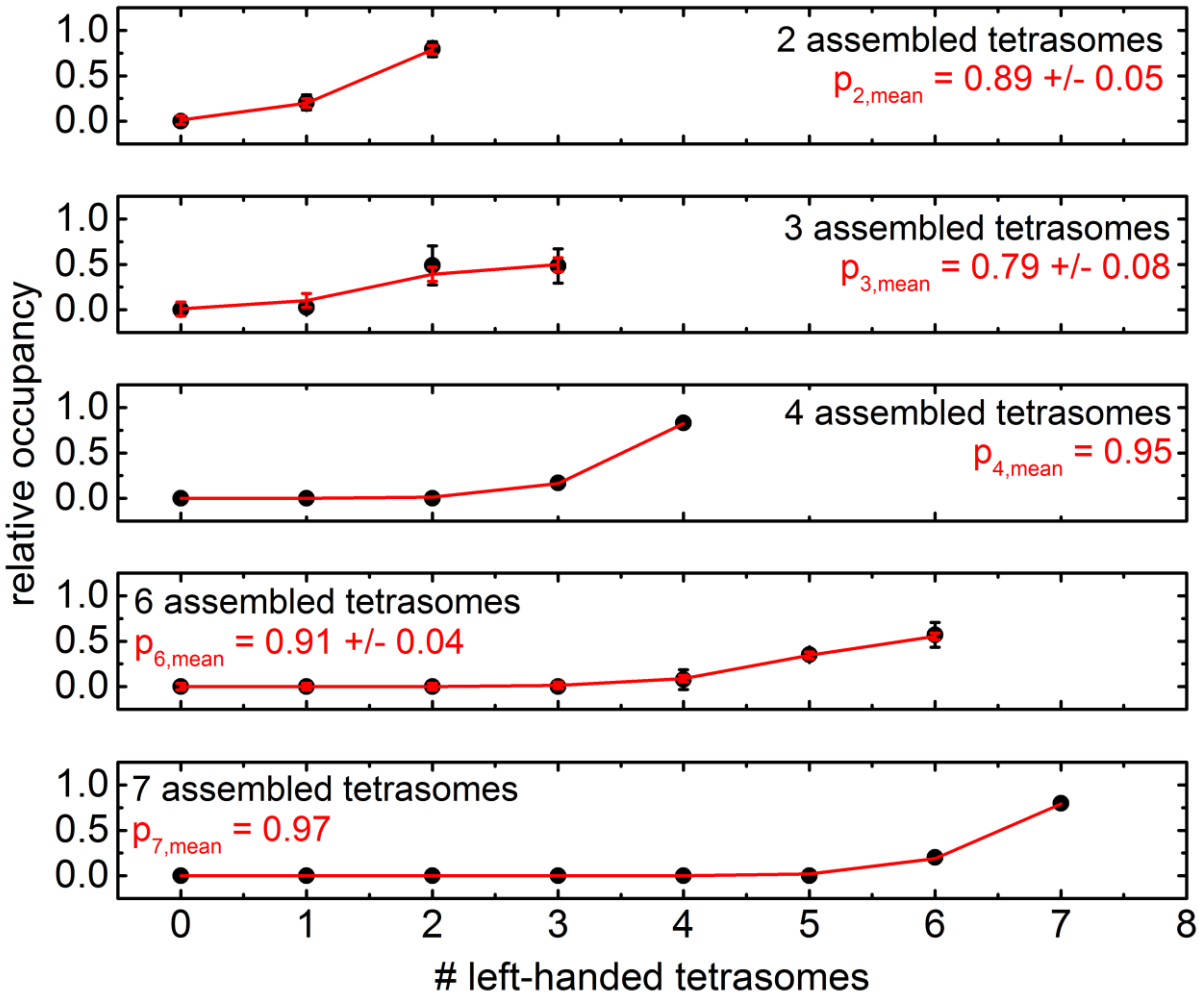

FIG. S14. Probability of a $(H3.3_{IA}\text{-}H4)_2$ tetrasome occupying the left-handed state. Relative occupancies are obtained from the ratios of the mean peak areas of the linking number distributions for different numbers of assembled, flipping $(H3.3_{IA}\text{-}H4)_2$ tetrasomes. Data sets displaying the same number of assembled tetrasomes were averaged (black circles), if applicable, and plotted together with a corresponding binomial curve (red line) generated using the mean value of the probabilities obtained from a binomial fit to each data set. Data sets displaying different number of assembled tetrasomes are presented in separate panels. Non-occupied states were assigned to the value of 0 relative occupancy. A mean probability of a $(H3.3_{IA}\text{-}H4)_2$ tetrasome occupying the left-handed state of p_{left} = 0.88 ± 0.08 was determined by averaging over all individual data sets.

SUPPLEMENTARY REFERENCES

1. Sobieszek, A., Matusovsky, O.S., Permyakova, T.V., Sarg, B., Lindner, H. and Shelud'ko, N.S. (2006) Phosphorylation of myorod (catchin) by kinases tightly associated to molluscan and vertebrate smooth muscle myosins. *Arch. Biochem. Biophys.*, **454**, 197-205.
2. Yu, Z.B., Dulin, D., Cnossen, J., Kober, M., van Oene, M.M., Ordu, O., Berghuis, B.A., Hensgens, T., Lipfert, J. and Dekker, N.H. (2014) A force calibration standard for magnetic tweezers. *Rev. Sci. Instrum.*, **85**, 9.
3. Cnossen, J.P., Dulin, D. and Dekker, N.H. (2014) An optimized software framework for real-time, high-throughput tracking of spherical beads. *Rev. Sci. Instrum.*, **85**, 10.
4. Lipfert, J., Wiggin, M., Kerssemakers, J.W.J., Pedaci, F. and Dekker, N.H. (2011) Freely orbiting magnetic tweezers to directly monitor changes in the twist of nucleic acids. *Nature Communications*, **2**, 9.
5. Vlijm, R., Lee, M., Lipfert, J., Lusser, A., Dekker, C. and Dekker, N.H. (2015) Nucleosome assembly dynamics involve spontaneous fluctuations in the handedness of tetrasomes. *Cell Rep.*, **10**, 216-225.